

博士論文番号: 1581204
(Doctoral student number)

Mechanism of the Membrane Binding of the F-BAR Domain Protein GAS7

Maisarah Ab Fatah
Nara Institute of Science & Technology
Graduate School of Biological Sciences
Molecular Medicine & Cell Biology Laboratory
(Prof Shiro Suetsugu)
6 September 2018

Table of Contents

1.0 Introduction	6
1.1 BAR domains	6
1.1.1 Classical BAR domains/N-BAR domains.....	7
1.1.2 I-BAR domains	8
1.1.3 F-BAR domains	9
1.2 GAS7 proteins	12
1.2.1 GAS7 protein structure.....	13
1.3 BAR proteins binding mechanism.....	15
2.0 Materials and Methods.....	17
2.1 Gene cloning.....	17
2.2 Protein expression.....	18
2.3 Protein purification	18
2.4 Preparation of GAS7 mutants.....	19
2.5 Cell cultures.....	26
2.6 Liposome preparations and liposome co-sedimentation assay.....	27
2.7 Preparation of PC:PS:PE-GUVs.....	27
2.8 Fluorescence microscopy	28
2.9 Transmission electron microscopy	28
2.10 Cryo-transmission electron microscopy.....	28
2.11 Crosslinking assays.....	29
2.12 Statistical analyses	30
3.0 Results.....	31
3.1 Binding activity of GAS7 isoforms to the liposomes	31
3.1.1 Liposome co-sedimentation assay	31
3.1.2 Transmission electron microscopy.....	34
3.1.3 GAS7b on the GUV	35
3.1.3.1 GFP-GAS7b on GUV	35

3.1.3.2 Cryo-transmission electron microscopy (cryo-EM) on GAS7b	35
3.2 Mutations on GAS7 F-BAR domain	36
3.2.1 Mutations of the GAS7 loops	37
3.2.2 FFL2 without protein contact interacts with membrane surface	43
3.2.3 The point mutants of the membrane binding surface and the dimer-dimer interaction (oligomerization)	47
3.2.4 The mutants that affect the stability of FFLs.....	49
3.2.5 Surface interaction mutant.....	53
3.3 Crosslinking assays.....	55
4.0 Discussions.....	59
5.0 Acknowledgments	68
6.0 References	69

Lab name (Supervisor)	Laboratory of Molecular Medicine & Cell Biology (Prof. Shiro Suetsugu)		
Name (surname) (given name)	Ab Fatah, Maisarah	Date	2018/09/06
Title	Mechanism of the Membrane Binding of the F-BAR Domain Protein GAS7		

Protein-lipid interactions play important roles in cell signaling, lipid metabolism, membrane trafficking and various other cellular processes. Bin-Amphiphysin-Rvs (BAR) domains are highly conserved and forms membrane curvatures. Extended Fes-CIP4 homology (EFC)/FCH-BAR (F-BAR) domain is one of the subfamilies in the BAR domain superfamily. The BAR domain proteins bind to membrane as homodimers, which then assemble into the ordered oligomer on the membrane. However, the ordered assembly of most BAR domains are unclear. Growth-Arrest-Specific-Protein-7 (GAS7) consists of the SH3 domain, the WW domain, and the F-BAR domain, dependent on the splicing isoforms. GAS7c has the SH3, WW, and F-BAR domains, GAS7b has WW and F-BAR domains, and GAS7a has F-BAR domain only. GAS7 is shown to be involved in neurite outgrowth, neuronal differentiation, phagocytosis, presumably through the membrane deformation through its F-BAR domain and the regulation of the actin cytoskeleton through its WW and SH3 domains.

In this study, I examined the ordered oligomer formation of GAS7 for its membrane binding. The membrane binding of GAS7 protein was examined by the liposome co-sedimentation assay. The co-sedimentation assay revealed all three isoforms have the ability to bind to liposomes made of bovine Folch fraction, a total fraction of the bovine brain lipids. The Folch fraction is rich in phosphatidylserine, a negatively charged phospholipids, and thus, the liposomes are negatively charged. Therefore, the GAS7 and the liposomes are thought to bind through the electrostatic interactions.

The binding and localization of GAS7 on liposomes of giant unilamellar vesicles (GUV) was observed by fluorescent microscope. Further, using cryo-electron microscope, I observed the striations on the GUV membrane in the presence of GAS7b, as compared to protein-free liposomes, indicating the ordered oligomer on the membrane.

The asymmetric unit of the GAS7 F-BAR domain crystals contained two F-BAR dimers, forming a shallow concave curvature. These dimers interact with symmetry-related dimers, forming two flat filamentous oligomers (FFO) in the crystals. The geometry of the striations on the surface of GUV had similar width and pitch with the FFO in the crystal, suggesting that FFO is the form of GAS7 for the membrane binding.

Two loops were involved in the FFO formations in the crystal. These loops are filament forming loop 1 (FFL1; aa 171-197) and filament forming loop 2 (FFL2; aa 206-219). In order to determine the roles of FFLs GAS7, I made the mutants with deletions of the FFLs. In HeLa cells, the membrane binding of GAS7 as FFO was indicated by the GAS7b localization, where GAS7 excluded the plasma membrane marker, suggesting that GAS7 assembles into patches of highly concentrated GAS7b on the plasma membrane. I expressed all these mutants in

HeLa cells and the mutants of FFL1 and FFL2 showed significantly reduced patches formation. This suggest that these two loops are involved in the patch formation in the HeLa cells. The *in vitro* membrane bindings of these deletion mutants were significantly decreased in the co-sedimentation assay. Therefore, the oligomer formation presumably through FFLs is involved in the membrane binding both *in vitro* and *in vivo*.

I mutated R326 residue, which have contacts with both N177 of FFL1 and D207 of FFL2, contributing the stability of the FFLs. When I substituted R326 to alanine, the patches in HeLa cells were significantly decreased. The oligomer formation *in vitro* was examined by the chemical cross-linkers, and the oligomer formation of R326A mutant was not efficient as GAS7b. However, the membrane binding was decreased but retained in the co-sedimentation assay. Therefore, GAS7 was thought to bind to the membrane independently of oligomer formation, and the oligomeric GAS7b had higher affinity to the membrane.

I also made another two mutants with the substitutions of the amino-acid residues on the surface of the FFO, that are Q212R and K370E/R374E, where the membrane is supposed to interact with. Q212 is located at the tip of one of the FFL2 that does not interact with the adjacent dimers in the FFO and is exposed to the surface of FFO. The Q212R mutant showed patches which is similar as the WT in HeLa cells. This mutant increased the membrane binding. Therefore, the surface of FFL2 without interaction with the adjacent GAS7 F-BAR dimer is suggested to be involved in the membrane binding. K370E/R374E mutant, which is located at the FFO surface, showed the reduction of the patch formation in HeLa cells. The K370E/R374E mutant with substitutions of positively charged amino-acid residues to negatively charged ones, decreased the binding between GAS7 proteins and liposomes, supporting the idea of the electrostatic interactions between the GAS7 and the membrane. These Q212 and K370/R374 mutations indicated that the surface formed by these amino-acid residues is the membrane binding surface.

Based on these data, I proposed that the oligomer assembly of GAS7 plays a role in the membrane binding. The interaction between dimers through FFL1 and FFL2 will assemble the F-BAR domains to form oligomers on the membrane surface, where the Q212, K370, and R374 residues locate on the membrane. When the assembly of these oligomers is hindered by the deletions, the formation of the protein oligomers on the membrane surface was also be inhibited, resulting in the reduced membrane binding activity, which was proven by co-sedimentation assay. The mutation of R326 might affect the location of the two FFLs, and thereby change the stability of the oligomer formation through the loops. This affects the oligomer formation in the cells and on the membrane, because the R326 mutant retained the membrane binding *in vivo* without the patch assembly in the HeLa cells, and cross-linking *in vitro*.

The F-BAR domain of PACSIN2 has the hydrophobic loops, which are inserted into the membrane, contributing to the membrane binding. The FFLs of GAS7 are hydrophilic and are not inserted into the membrane to form membrane curvature. The FFLs contribute to the formation of oligomers that can further assemble into sheets along the membrane surface. These findings have given an insight on how GAS7 assembly works on the membrane.

1.0 Introduction

1.1 BAR domains

Living cells are surrounded by membrane. The formation of membrane curvature during large numbers of cellular processes is important as it leads to the formation of the complexed intracellular architectures, which are necessary for most of cellular organelles to function. Among them are endocytosis, phagocytosis, exocytosis, and migration. In these processes, the generation of membrane curvature is supposed to be coupled with the spatial distribution of proteins and lipids (Zimmerberg and Kozlov, 2006; Meer *et al.*, 2008; Suetsugu *et al.*, 2014; Simunovic *et al.*, 2015; Nishimura *et al.*, 2018). This membrane curvature formation is known to be sensed and/or generated by a group of proteins, known as the BAR (Bin-Amphysin Rvs167) domain superfamily (Itoh and Camilli, 2006; Frolov and Zimmerberg, 2008; Frost *et al.*, 2009; Nishimura *et al.*, 2018). The BAR domains consist of dimeric α -helical coiled-coils that bind to acidic membrane phospholipids and induce or stabilize membrane curvatures to achieve specific shapes that correspond to their membrane-binding surfaces (Peter *et al.*, 2004). Each BAR protein contains BAR domain that usually varies in length, intrinsic curvature, and also the binding affinity towards the membrane. The dimeric BAR domains further homo-oligomerize, forming the spiral-like wrapping of the membrane. The homo-oligomer, as well as dimer structure of each BAR domain is thought to function as scaffold for membrane curvature sensing or generation. All BAR domains are thought to be able to form this membrane scaffold. BAR domain composed of an alpha-helix bundle is harder than membrane, and thus can bend membrane, which is formed by the hydrophobic interactions between lipid molecules.

There are three subfamilies under the BAR domain superfamily, which are known as the classical BAR domains including N-BAR domains (N-terminal amphipathic helix BAR), the I-BAR (Inverse BAR) domains, and the F-BARs (Fes/CIP4 Homology-BAR) domains (Habermann, 2004; Peter *et al.*, 2004; Itoh and Camilli, 2006; Frost *et al.*, 2007; Suetsugu *et al.*, 2010; Safari and Suetsugu, 2012; Liu *et al.*, 2015). All BAR domains consist of α -helix bundle. All of these domains are structurally similar homodimeric modules of antiparallel arrangement of monomers, exhibiting similar banana- or zeppelin-like structure, but with different overall curvature (Figure 1). This leads to different preferences to membrane curvature (Habermann, 2004; Peter *et al.*, 2004; Itoh and Camilli, 2006; Henne *et al.*, 2007; Daumke *et al.*, 2014; Simunovic *et al.*, 2015; Suetsugu *et al.*, 2010).

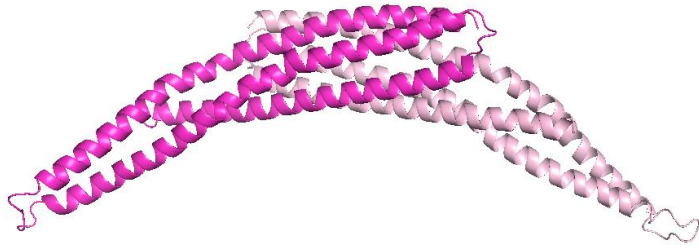
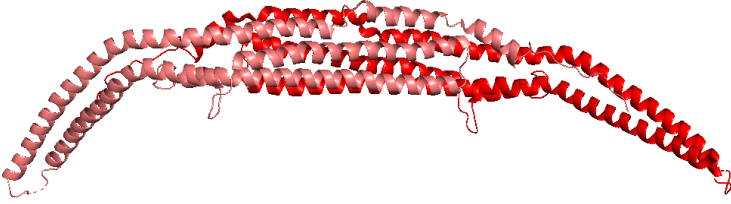
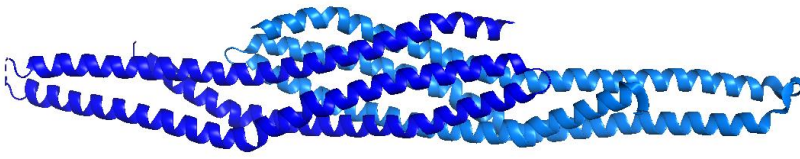
BAR Domain	Protein structure
N-BAR	 <p data-bbox="842 629 912 663">BIN2</p>
F-BAR	 <p data-bbox="810 965 940 999">PACSIN2</p>
I-BAR	 <p data-bbox="826 1256 924 1290">IRSp53</p>

Figure 1: Human BAR domain superfamily proteins.

1.1.1 Classical BAR domains/N-BAR domains

Most of the classical BAR domain-containing proteins (BAR proteins) have an amphipathic helix that usually reside in the N-terminus (Peter *et al.*, 2004). The amphipathic helices prefer steep curvature, because this geometry promotes a high concentration of lipid-packing defects, sensed by amphipathic motifs. Some BAR domain possesses the amphipathic helices at their N-terminus, and thus called as N-BAR domain (Gallop *et al.*, 2006; Campelo *et al.*, 2009). BAR proteins are able to generate tubules that exhibit positive curvature, i.e., the concave surface of the BAR domains binds to the membrane. Their tubules size ranges from approximately 20 nm to 60 nm wide (Peter *et al.*, 2004).

Among the proteins that are categorized under the N-BAR domain are amphiphysin, Bin and endophilin (Cui *et al.*, 2009; Arkhipov *et al.*, 2009; Safari and Suetsugu, 2012) (Figure

2). N-BAR protein endophilin plays role in endocytosis, a process by which cells internalize extracellular materials. When bound to membrane tubules, the amphipathic helices of endophilin penetrates deeper into the bilayer. The N-terminal amphipathic helix of the endophilin BAR domain increased the affinity for membrane lipids, while the crescent-shaped dimeric BAR domain itself was vital for membrane tubulation (Gallop *et al.*, 2006, Yin *et al.*, 2009; Chen *et al.*, 2016).

The difference of the N-BAR domain concentration was able to formed three types of curved membrane structures when were introduced in liposomes. It had been suggested that helices are responsible for curvature sensing at low protein concentration, whereas the BAR domain plays role in controlling membrane curvature at high concentration (Isas *et al.*, 2015). At low concentration, small buds were formed; elongated tubules were formed at intermediate concentration while vesicles were formed at high concentrations (Ayton *et al.*, 2007; Ayton *et al.*, 2009; Suetsugu and Gautreau, 2012; Salzer *et al.*, 2017). But this action of the N-BAR domain would be applicable to all of the BAR domains.

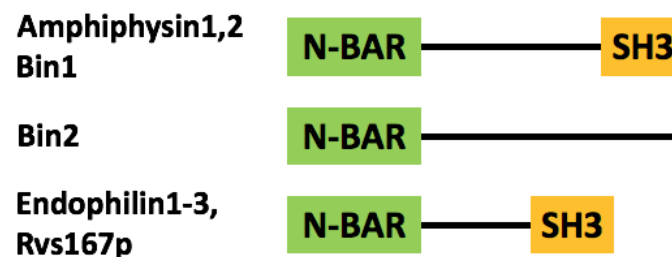


Figure 2: Domain schematic of N-BAR domain proteins.

1.1.2 I-BAR domains

The I-BAR domain consists of three α -helices and form dimers. It is less curvy as compared to classical BAR. Clusters of positively charged amino acids that resides at their convex surface, rather than the concave side as in other BAR and F-BAR domains. Therefore, the I-BAR domain is involved in the membrane curvature that is in the opposite direction as compared to those by the other BAR proteins. This curvature is known as negative membrane curvature. The I-BAR domains bind to phosphoinositides-rich membrane, mainly through electrostatic interactions (Suetsugu *et al.*, 2006a; Mattila *et al.*, 2007). There are five known I-BAR domain-containing proteins in vertebrates (Scita *et al.*, 2008); IRSp53 (insulin receptor phosphotyrosine 53 kDa substrate), IRTKS (insulin receptor tyrosine kinase substrate), Pinkbar, MIM (Missing-in-Metastasis), and ABBA (Another B-box Affiliate) (Figure 3). All these proteins contain an N-terminal I-BAR domain, and C-terminal WH2-like domain, with different isoforms. I-BARs

such as ABBA and MIM contain amphipathic helices, but not in IRSp53, IRTKS, and Pinkbar. These amphipathic helices are inserted into the membrane during membrane curvature. I-BAR was reported to be involved in the formation of filopodium (Lim *et al.*, 2008) and lamellipodium formation such as neurite extension (Govind *et al.*, 2001), dendritic spine morphogenesis (Abbott *et al.*, 1999; Soltau *et al.*, 2002; Soltau *et al.*, 2004; Choi *et al.*, 2005) and tumor invasiveness (Suetsugu *et al.*, 2006b; Liu *et al.*, 2010; Robens *et al.*, 2010).

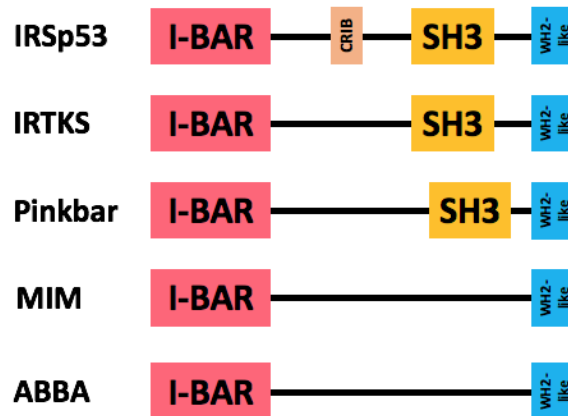


Figure 3: Domain schematic of I-BAR domain proteins.

1.1.3 F-BAR domains

The F-BAR domains are characterized by having long and shallow BAR domains. They also form positive curvature, but with wider tubules, ranging from approximately 60 nm to 100 nm (Shimada *et al.*, 2007; Itoh and Camilli, 2006; Frost *et al.*, 2008; Qualmann *et al.*, 2011). There are more than 10 proteins that are categorized as F-BAR domain. Among them are FCHO, Syndapin/PACSIN, NOSTRIN, GAS7, CIP4, FBP17 and PSTPIP (Ahmed *et al.*, 2010; Safari and Suetsugu, 2012) (Figure 4).

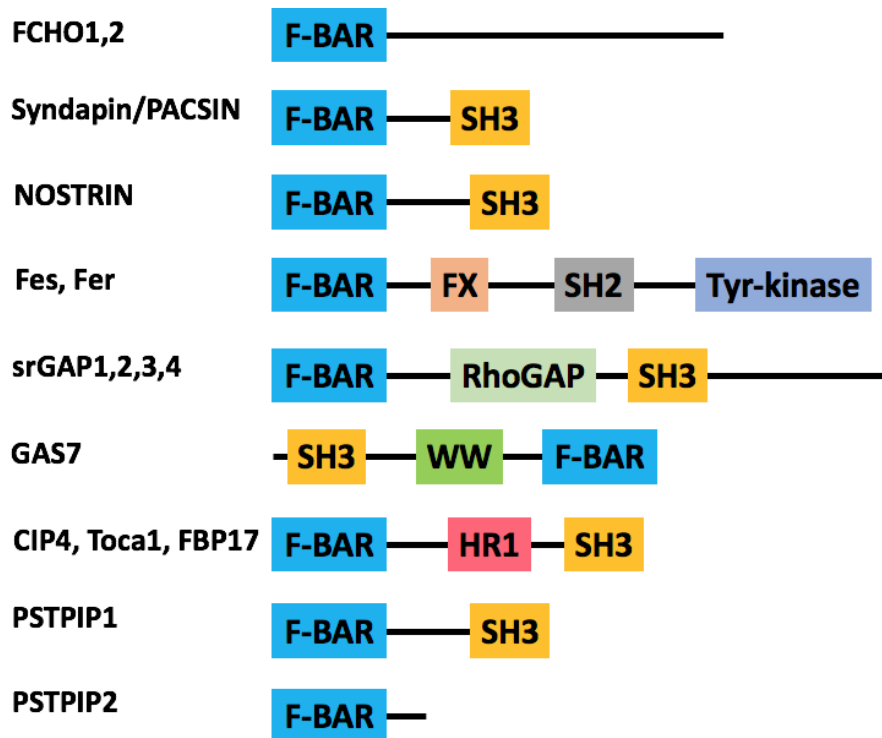


Figure 4: Domain schematic of F-BAR domain proteins.

The F-BAR proteins are mostly found in eukaryotes, except in plants (Heath and Insall, 2008). Most of the known F-BAR proteins were involved in clathrin-mediated or caveolin-dependent endocytosis (Henne *et al.*, 2010). However, the involvements in the formation of filopodia; formation of axon; and lamellipodia; inhibition of axon formation are reported for some of the F-BAR proteins. CIP4 is the first F-BAR domain with structural determination (Shimada *et al.*, 2007). It consists of five α -helices; the short N-terminal helix, three long and one short C-terminal helices (Figure 5a). Helices α_2 , α_3 and α_4 form an intimately packed, six-helix bundle with a neighboring symmetry-related molecule, which results in a gently curved dimer (Figure 5b) (Shimada *et al.*, 2007). The shapes of the CIP4 F-BAR domain are quite complementary, binds tightly to the curved membrane by accumulating at the foot of the nascent tubular membrane to form membrane tubulation (Figure 5c) (Shimada *et al.*, 2007).

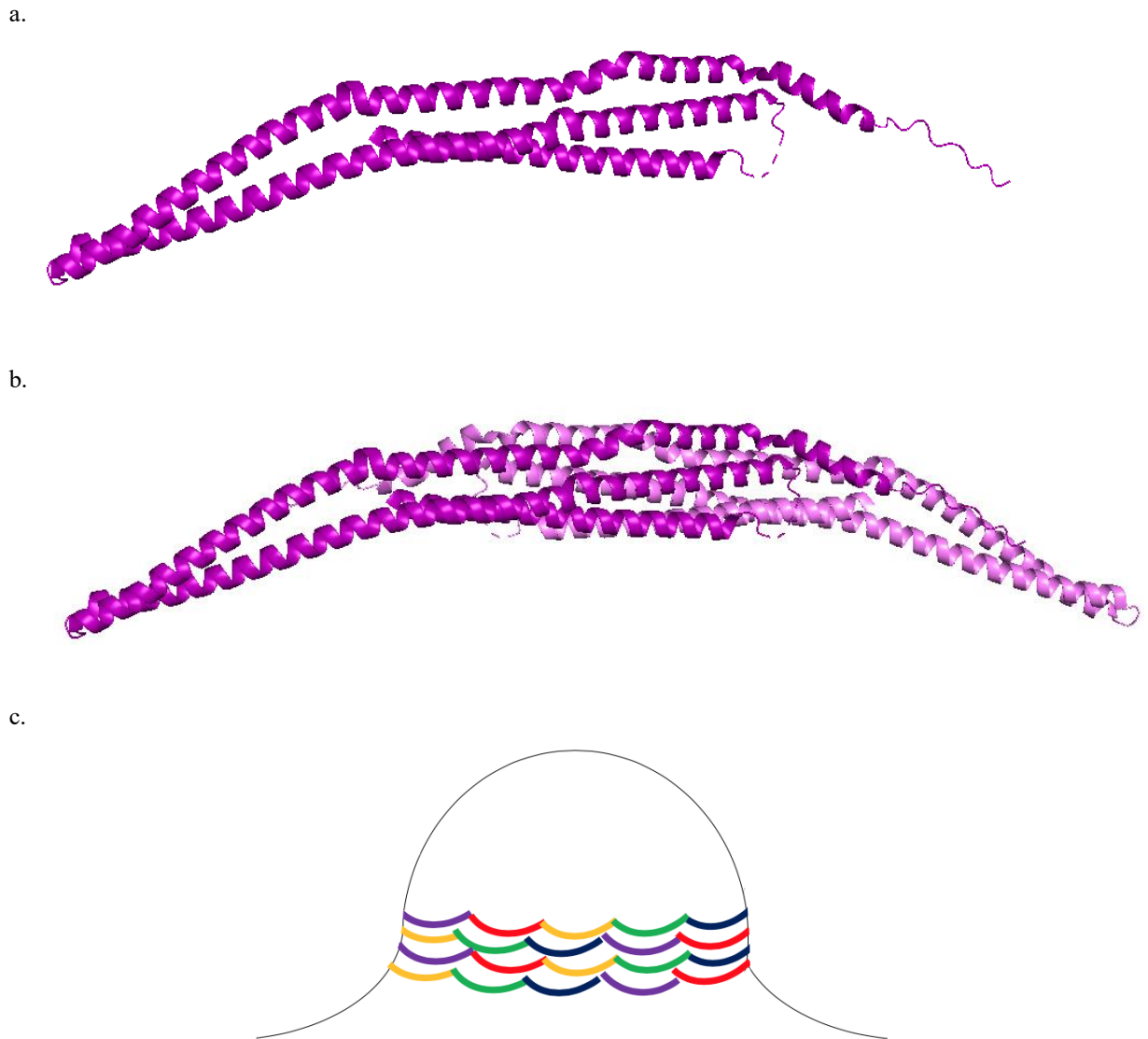


Figure 5: Ribbon diagrams of the crystal structure of CIP4 F-BAR domain, consisting of five α -helices; the short N-terminal helix, three long and one short C-terminal helices. (a) Monomeric form is shown, but it functions as dimer. Broken lines indicate regions that could not be modeled. (b) The dimer form of CIP4, forming a shallow concave curvature. (c) Schematic illustration showing how the CIP4 F-BAR domain tubulates the lipid membrane from a liposome. Each dimer is colored differently.

PACSIN, which is also known as syndapin, consists of three isoforms named PACSIN1, PACSIN2 and PACSIN3. All PACSIN consists of N-terminal F-BAR domain and a C-terminal SH3 domain. PACSIN1 and PACSIN2 have hydrophobic wedge loop, which is known to facilitate the membrane curvature (Qualmann and Kelly, 2000; Shimada *et al.*, 2010) (Figure 6). Another F-BAR protein, PSTPIP, consists of two members, which are PSTPIP1 and PSTPIP2. PSTPIP1 has an N-terminal F-BAR domain, PEST motifs (peptide sequence rich in proline, glutamic acid, serine and threonine) and a C-terminal SH3 domain. However, PSTPIP2

does not contain PEST motifs and SH3 domain (Spencer *et al.*, 1997; Wu *et al.*, 1998a; Wu *et al.*, 1998b; Li *et al.*, 1998).

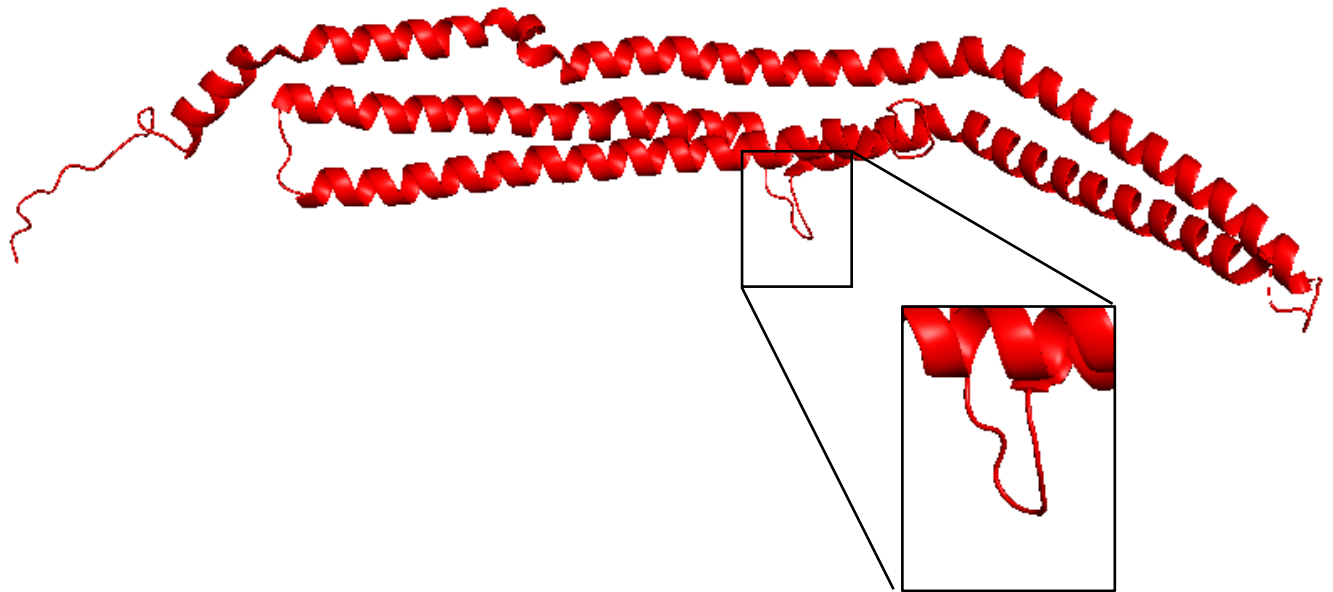


Figure 6: Ribbon diagrams of the PACSIN2 F-BAR domain crystal structure of PACSIN2 F-BAR domain, consisting of a short wedge loop (insert).

1.2 GAS7 proteins

Growth-Arrest-Specific 7 proteins (GAS7) are one of the F-BAR proteins. GAS7 is mostly found in early embryonic cells, testis and neurons of mouse brain; which includes cerebral cortex, hippocampus, and cerebellum (She *et al.*, 2002; Chang *et al.*, 2005; You *et al.*, 2010; Hidaka *et al.*, 2012; Tseng *et al.*, 2015). Tseng *et al.* (2015) reported that lower expression of GAS7c promotes metastasis in lung cancer. GAS7 is necessary for neuronal differentiation. GAS7 also interacts directly with actin to promote its assembly and F-actin into bundles to form oligomers through its F-BAR domain (Gotoh *et al.*, 2013).

It is important to know how GAS7 F-BAR domain organization and assembly works in generating membrane curvature. There are three GAS7 isoforms; GAS7a, GAS7b and GAS7c in Homo sapiens. In GAS7c, there are the Src-homology 3 domain (SH3), the WW domain, and the F-BAR domain, from N-terminus to C-terminus. The SH3 domain is only present in GAS7c, while GAS7a only consists of the F-BAR domain (Figure 7).

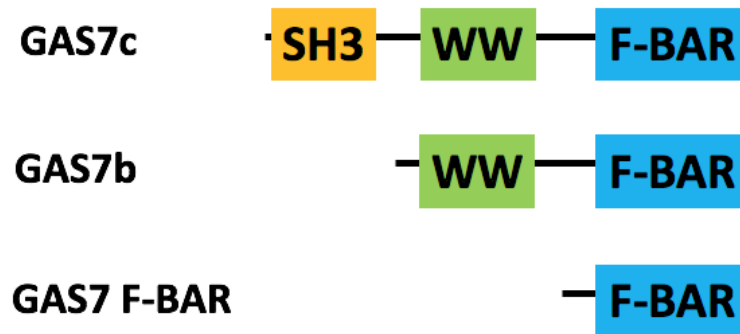


Figure 7: Domain schematic of GAS7 isoforms.

The SH3 domain is able to bind to the proline-rich ligands, regulating their subcellular localization and their enzymatic activities. In Syndapin/PACSIN, the SH3 domains bind to dynamin and N-WASP, and were shown to bind to the membrane interaction site of the BAR domain, thus auto-inhibiting the scaffold assembly and/or membrane remodeling (Rao *et al.*, 2010). The similar auto-inhibition has been suggested for endophilin (Chen *et al.*, 2014) and amphiphysin; but the mechanistic details in amphiphysin was not clear.

The lengths of WW domains are approximately 40 amino acids, making it the smallest naturally occurring protein modules. The WW domain is characterized by two tryptophan (W) residues, that are spaced 20-22 amino-acids residues apart (Macias *et al.*, 2002). The WW domains can be found in cytoplasm and in cell nucleus. The WW domain also recognizes proline-containing ligands by a three-stranded, antiparallel β -sheet, with two ligand-binding grooves (Chong *et al.*, 2006). The proteins containing the WW domain are involved in variety of cellular process such as protein trafficking, RNA processing, receptor signaling and transcription (Ingham *et al.*, 2005). The WW domain in GAS7 was reported to be associated with Neural-Wiskott Aldrich syndrome protein (N-WASP) and heterogeneous nuclear ribonucleoprotein U (hnRNP U). The interaction with N-WASP is thought to actin nucleation (Tseng *et al.*, 2015).

1.2.1 GAS7 protein structure

The crystal structure of the GAS7 BAR domain was determined by from Medical Institute of Bioregulation, Kyushu University. The asymmetric unit of the GAS7 F-BAR domain crystals contained two F-BAR dimers (Hanawa-Suetsugu *et al.*, unpublished results, PDB code 5YM1), forming a shallow concave curvature (Figure 8). These dimers interact with symmetry-related dimers, forming two flat filamentous oligomers (FFO) in the crystals (Figure 8c). The F-BAR dimers are 22 nm in length, and FFOs have a width of ~14 nm. The spacing between adjacent

F-BAR dimers in FFOs was ~ 5 nm (Figure 8c). GAS7 consists of two loops. These two loops were involved in the FFO formations in the crystal. These loops are filament forming loop 1 (FFL1; aa 171-197) (Figure 8a, blue) and filament forming loop 2 (FFL2; aa 206-219) (Figure 8a, magenta) from the crystal packing.

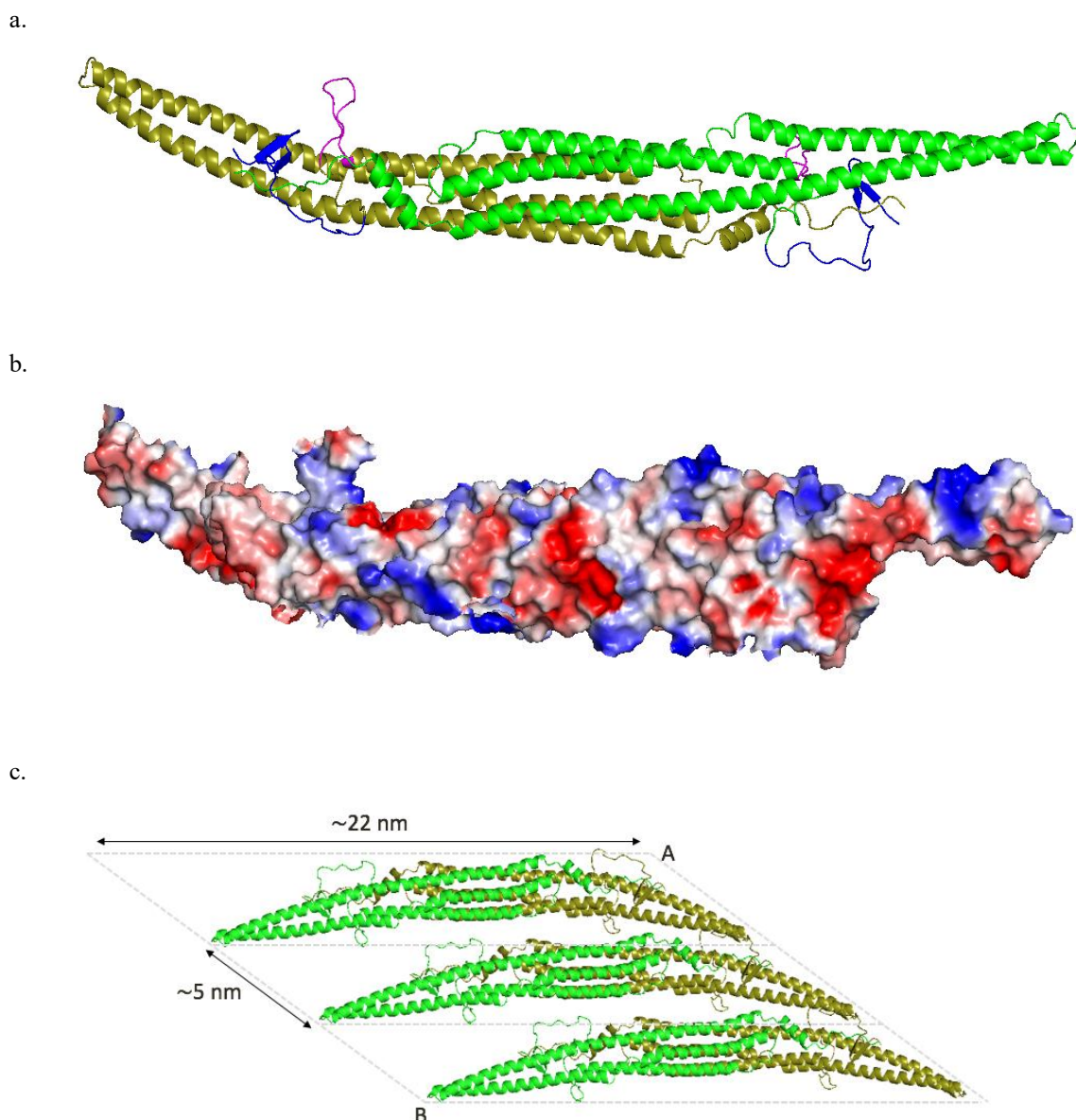


Figure 8: (a) Ribbon diagrams of the crystal structure of GAS7 F-BAR domain, consisting of two dimers, forming a shallow concave curvature. FFL1 was indicated by blue, while FFL2 was indicated by magenta. (b) Electrostatic potential surfaces of the GAS7 F-BAR dimers. Blue and red indicate positive and negative charges, respectively. (c) The asymmetric unit of the crystal contains two F-BAR dimers, both of which form an FFO. The F-BAR dimers are 22 nm in length, and FFOs have a width (diagonal measurement from point A to point B) of ~ 14 nm. The spacing between adjacent F-BAR dimers in FFOs was ~ 5 nm.

1.3 BAR proteins binding mechanism

In order to sense/generate curvature on the membrane, the BAR domain dimers will assemble on the membrane into higher-order oligomers. The size of membrane tubules and cellular organelles are generally larger than protein size. Therefore, higher-order assembly is required to shape membranes, so that the BAR domain protein filaments are able to form decorations on the membrane surface and ‘wrap up’ (as shown in Figure 5c) part of the subcellular organelles (Shimada *et al.*, 2007; Suetsugu, 2016). When the BAR domains are recruited to membrane, BAR domain dimers are thought to self-assemble through the low-affinity interactions between the BAR domains (Frost *et al.*, 2008). Besides that, BAR domains bind to the membrane through electrostatic interactions, where the membrane binding is mostly based on the interaction between positively charged amino acids of the proteins and negatively charged lipids, such as phosphatidylserines and phosphoinositides.

There are two studies that examined the detailed interactions between BAR or F-BAR domains on the membrane (Shimada *et al.*, 2007; Frost *et al.*, 2008). CIP4 F-BAR domain uses lateral contacts and tip-tip interaction of their F-BAR domains to form helical oligomers at tubular membrane surface (Shimada *et al.*, 2007; Frost *et al.*, 2008). On the other hand, the N-BAR protein, endophilin, bends the membrane by inserting an N-terminal amphipathic helix and internal amphipathic helix into the phospholipids bilayer, and wrap the membrane through the alignments of the BAR domains with amphipathic helices between the BAR domains (Mim *et al.*, 2012) (Figure 9). The N-BAR domain of endophilin is made of three membrane binding sites; an N-terminal amphipathic helix, a BAR monomer and an internal amphipathic helix and additional loop sequences. Insertion of both amphipathic helix; i.e. the N-terminal and internal helices; promotes curvature. At the same time, dimerization of the BAR stabilizes the protein on the membrane. Once the curvature was initiated, the energetic barriers for further N-BAR domain recruitment will be lower, thus resulting in a scaffolding of the curvature (Gallop *et al.*, 2006).

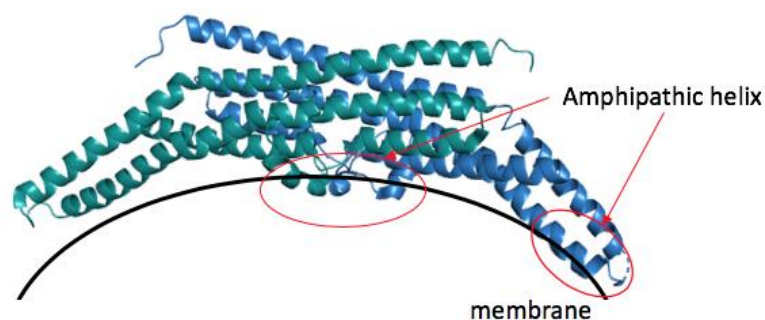


Figure 9: Illustration on how Endophilin N-BAR binds to the membrane.

Among the F-BAR domains, PACSIN1/2 has the loops that are inserted into the membrane (Wang *et al.*, 2009; Shimada *et al.*, 2010; Senju *et al.*, 2011). Although the detailed assembly had not been determined, PACSIN1 and PACSIN2 F-BAR domains were very similar, and resembles the structure of other F-BAR domains such as CIP4, FBP17 and FCHo2 (Wang *et al.*, 2009). PACSIN F-BAR domain has a unique, 8-residues-long insertion in helix 2 of PACSIN that forms a flexible loop in the crystal structure, which was proposed to have an equal function to an amphipathic helix and work as a wedge for membrane bending. This loop is known as the wedge loop, and are inserted into the membrane to help in membrane curvature formation (Figure 10).

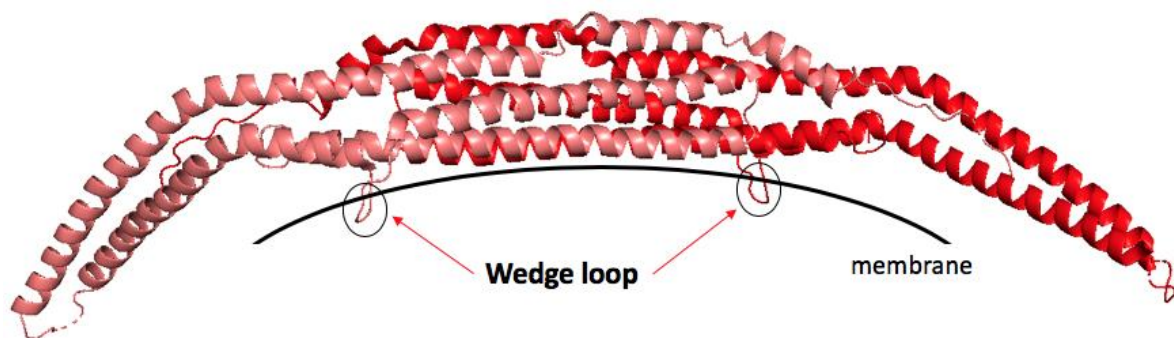


Figure 10: Illustration shows on how the wedge loops in PACSIN2 are inserted into the membrane, which helps membrane curvature.

Since the GAS7 F-BAR domain crystal structure was just revealed, the studies of this structure have not yet been investigated. Hence, the function of the two loops in the GAS7 F-BAR domain crystal structure in the mechanism of membrane binding is still unknown. Thus, my main objective for this study is to determine the mechanism of the assembly of the GAS7 dimers on membrane surfaces. I will specifically examine the importance of the characteristic loops of GAS7 for the membrane binding and the assembly of GAS7 on the membrane, because the loops are mostly involved in the membrane insertion in the other BAR and F-BAR domains.

2.0 Materials and Methods

2.1 Gene cloning

The EGFP-C1-GAS7c, EGFP-GAS7b and EGFP-GAS7 F-BAR (Figure 11) were subcloned into pGEX6P-1 vector by Gibson assembly, using the EcoRI as the restriction site. The mixture of the template, the insert and the Gibson Assembly[®] Master Mix (New England Biolabs[®]), were incubated at 50°C for 1 hour (h), followed by transformation into JM109 competent cell. In order to screen for plasmids containing the desired insert directly from the bacterial colonies, I performed colony polymerase chain reaction (PCR) using EmeraldAmp[®] PCR Master Mix (Takara Bio). The PCR was carried out according to the manufacturer's protocol. The denaturing step was carried out at 98°C for 10 seconds (s), followed by annealing step at 55°C for 30 s and extending step at 72°C for 3.5 minutes (min). The cycle was repeated 25 times. Once the plasmids with the desired insert were confirmed, I amplified the targeted plasmids by carrying out PCR using the Prime STAR[®] MAX DNA Polymerase (Takara Bio). The templates and the primers were listed in Table 1. The PCR was carried out according to the manufacturer's protocol. The denaturing step was carried out at 98°C for 10 s, followed by annealing step at 53°C for 15 s and extending step at 72°C for 2 min. The cycle was repeated 35 times. The plasmids were then transformed using competent cell, JM109. After overnight pre-culture, the bacterial culture was purified by using Wizard[®] Plus SV Minipreps DNA Purification System (Promega), and the plasmids were sequenced to confirm the DNA sequence of desired construct. EGFP-CIP4 F-BAR was constructed and used as the positive control in the initial part of this project.

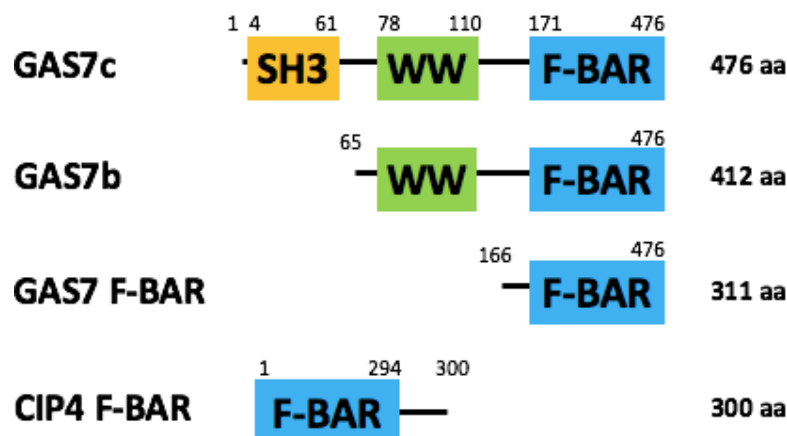


Figure 11: The GAS7 isoforms and CIP4 F-BAR used in this experiment.

2.2 Protein expression

The *E. coli* strain Rosetta-gami B was transformed with the expression plasmid for EGFP-GAS7c, EGFP-GAS7b and EGFP-GAS7 F-BAR. The cells were cultured in 500 ml of LB medium containing 0.034 mg/ml of chloramphenicol and 0.1 mg/ml of ampicillin at 37°C. When the absorbance at 600 nm (OD₆₀₀) reached between 0.6 and 0.7, the protein expression was induced with 0.02 mM Isopropyl β-D-1-thiogalactopyranoside (IPTG), and the cells were cultured overnight for 18-20 h, at 20°C. The bacterial pellet was then collected, stored at -80°C, and proceeded with purification.

2.3 Protein purification

The bacterial pellets from 100 ml culture were re-suspended in 1 ml of buffer containing 20 mM Tris-HCl (pH 7.5), 0.80 M NaCl, 10% glycerol, 1 mM DTT, and 1 mM phenylmethanesulfonyl fluoride or PMSF, and were disrupted with an ultrasonic homogenizer. The sonication was done for a total of 3 min, with 3 s of working period, and 3 s of resting period, at a tune of 6. After removing undisrupted cells from the crude extracts by centrifugation (15,000 rpm, 10 min, 4°C), the supernatant was transferred to 0.1 ml of Glutathione Sepharose 4B (GE Healthcare). Prior to the mixing of Glutathione Sepharose 4B beads with the supernatant, Glutathione Sepharose 4B was prepared by washing with the binding buffer (10 mM Tris-HCl pH 7.5, 150 mM NaCl, and 1 mM EDTA). The beads of Glutathione Sepharose 4B were centrifuged at 500 x g for 5 min at 4°C. This step was repeated a total of five times, with the volume of binding buffer 100 times the volume of Glutathione Sepharose 4B. Then, about 0.7 ml of the supernatant was added to 0.1 ml of prepared Glutathione Sepharose 4B, and were incubated for 1 h, at 4°C by using end-over-end rotation. After the rotation, the supernatant was carefully removed and the Glutathione Sepharose 4B, and the supernatant was collected for analysis of the protein binding to the beads. The beads were washed with 1 ml of the same binding buffer, mixed and centrifuged at 500 x g for 5 min at 4°C. This step was repeated five times, with the volume of binding buffer 10 times the volume of Glutathione Sepharose 4B beads. The bound protein was cleaved by adding 1.5 ul of GST Precision Protease (GE Healthcare) (10 mM Tris-HCl pH 7.5, 150 mM NaCl, 1 mM EDTA, 20% glycerol and 1 mM DTT) in 0.25 ml of binding buffer, and was incubated 16-18 h, at 4°C by using end-over-end rotation. After the incubation, this mixture was centrifuge at 500 x g for 5 min at 4°C. The supernatant (the eluted protein) was carefully removed and the protein concentration was measured by sodium dodecyl sulfate polyacrylamide gel electrophoresis (SDS-PAGE).

The same procedures were also used for untagged-GAS7 isoforms; GAS7c, GAS7b and GAS7 F-BAR proteins, and for the mutants.

2.4 Preparation of GAS7 mutants

Mutations were introduced by site-directed mutagenesis. Several amino acids residues on the loop and at the tip of the adjacent dimers were mutated to alanine, glutamic acid, arginine, proline or serine by using QuickChangeTM protocol as follows. The denaturing step was carried out at 98°C for 10 s, followed by annealing step at 53°C for 15 s and extending step at 72°C for 2 min. The cycle was repeated 35 times. 0.5 µl of Dpn1 was added after the amplification and the plasmids were incubated at 37°C for 1 h, and was proceeded with transformation. The mutagenic oligonucleotide primers used in this method were designed individually according to the desired mutations. Both mutagenic primers contain the mutation and anneal to the same sequence on opposite strands of the plasmid. The primers were between 25 and 45 bases in length, with a melting temperature of $\geq 78^\circ\text{C}$, as shown in Table 1. The desired mutation was in the middle of the primer, with ~10-15 bases of correct sequence on both sides. The selections of the mutants were based on the interactions between dimers from the structural analysis. There were 35 mutants that were introduced to GFP-GAS7b and EGFP-GAS7 F-BAR. Primers that were designed for the mutations were purchased from Hokkaido System Science Co., Ltd (Table 1). All the plasmid constructed were listed in Table 2. All these mutations were located at a conserved region of F-BAR domain (Figure 12).

Table 1: Primers used for QuickChangeTM modification. Red letters indicate the point of mutations.

Primer Name	Forward /reverse	Mutation	Sequence (5'-3')
GAS7MsdelK20 9-T216	Forward	Δ 209-216	ACTACTTTTGGGCGGACAAGGGTGGCTG GCTTTGAACTGCT
GAS7MsdelK20 9-T216	Reverse	Δ 209-216	AGCAGTTCAAAGCCAGCCA CCTTGTC GCCCAAAGTAGT
GAS7MsK209E	Forward	K209E	ACTTTTGGGCGGACAAGGAAGACCCA CAAGGCAATGGCAC
GAS7MsK209E	Reverse	K209E	GTGCCATTGCCTTGTGGGTCTTCCTTGT CCGCCAAAAGT

GAS7MsQ212R	Forward	Q212R	CGGACAAGAAGGACCCAC CGGGG CAAT GGCACGGTGGCTGG
GAS7MsQ212R	Reverse	Q212R	CCAGCCACCGTGCCATTGCC CCG TGGG TCCTTCTTGTCCG
GAS7Ms_del171_197s	Forward	Δ171-197	CAGGCAGGAAACAGAGCAA GTGG GAGC TACTGTGACTACTT
GAS7Ms_del171_197as	Reverse	Δ171-197	AAGTAGTCACAGTAGCTCC ACTT GCTC TGTTTCCTGCCTG
GFP_GAS7Ms_del171_197s	Forward	GFP Δ171-197s	GATCCAGGAAACAGAGCAA GTGG GAGC TACTGTGACTACTT
GFP_GAS7Ms_del171_197as	Reverse	GFP Δ171-197s	AAGTAGTCACAGTAGCTCC ACTT GCTC TGTTTCCTGGATC
GAS7Ms_E221As	Forward	E221A	CACGGTGGCTGGCTTTG CACTG CTGCT GCAGAAGC
GAS7Ms_E221As	Reverse	E221A	GCTTCTGCAGCAGCAGT GCAA AGCCAG CCACCGTG
GAS7Ms_R242Es	Forward	R242E	GAGATGTCCGAGTTCATC GAGG AAAG GATAAAGATTGAAG
GAS7Ms_R242Es	Reverse	R242E	CTTCAATCTTTATCCTTT CTC GATGAA CTCGGACATCTC
GAS7Ms_D319As	Forward	D319A	GACATGAAAAAGTGCG CCC ACCACAT CGCTGAC
GAS7Ms_D319As	Reverse	D319A	GTCAGCGATGTGGTGG CGC ACTTTTT CATGTC
GAS7Ms_R326As	Forward	R326A	CACCACATCGCTGACCTC GCTA AGCAG CTGGCGAGCCGCT
GAS7Ms_R326As	Reverse	R326A	AGCGGCTCGCCAGCTGCTTA GCG AGGT CAGCGATGTGGTG
R326Ds	Forward	R326D	CACCACATCGCTGACCTC GATA AGCAG CTGGCGAGCCGC
R326Das	Reverse	R326D	GCGGCTCGCCAGCTGCTTA TCG AGGTC AGCGATGTGGTG
K327As	Forward	K327A	CACATCGCTGACCTCCGT GCGC AGCTG GCGAGCCGCTATG

K327Aas	Reverse	K327A	CATAGCGGCTCGCCAGCTGCGCACGGA GGTCAGCGATGTG
K327Ds	Forward	K327D	CACATCGCTGACCTCCGTGAGCAGCTG GCGAGCCGCTATG
K327Das	Reverse	K327D	CATAGCGGCTCGCCAGCTGCTCACGGA GGTCAGCGATGTG
GAS7Ms_E351As	Forward	E351A	GAGCGGCAGAAAGACCTGGCGATGAA GACCCAGCAGCTGG
GAS7Ms_E351As	Reverse	E351A	CCAGCTGCTGGGTCTTCATCGCCAGGT CTTTCTGCCGCTC
GAS7Ms_H431A_M435As	Forward	H431A/M43 5A	CACACAGCTGCGGGCCGAGACGGACG CGTTCAACCAAAGCA
GAS7Ms_H431A_M435As	Reverse	H431A/M43 5A	TGCTTTGGTTGAACGCGTCCGTCTCGG CCCGCAGCTGTGTG
GAS7Ms_Q438As	Forward	Q438A	GAGACGGACATGTTCAACGCAAGCAC AGTCGAGCCTGTGG
GAS7Ms_Q438As	Reverse	Q438A	CCACAGGCTCGACTGTGCTTGCGTTGA ACATGTCCGTCTC
GAS7Ms_R449As	Forward	R449A	CCTGTGGACCAACTGCTGGCAAAAAGTG GACCCAGCCAAAG
GAS7Ms_R449As	Reverse	R449A	CTTTGGCTGGGTCCACTTTTGCCAGCA GTTGGTCCACAGG
Gas7Ms_W397S	Forward	W397S	CAACCAGGCCAGTCCAAGTCGTTTGA AGAGATGGTGACGACC
Gas7Ms_W397S	Reverse	W397S	GGTCGTCACCATCTCTTCAAACGACTT GGACTGGGCCTGGTTG
Gas7Ms_W460S	Forward	W460S	GCCAAAGACAGAGAGCTATCGGTCAG AGAGCACAAAACAG
Gas7Ms_W460S	Reverse	W460S	CTGTTTTGTGCTCTCTGACCGATAGCTC TCTGTCTTTGGC
GAS7N177Ps	Forward	N177P	GAAAACACCATCACCATCCCTGTGTG ACATTCCCTCACCC
GAS7N177Pas	Reverse	N177P	GGGTGAGGGAATGTCACACAGGGGAT GGTGATGGTGTTC

D207Rs	Forward	D207R	GTGACTACTTTTGGGCG CG CAAGAAGG ACCCACAAGGC
D207Ras	Reverse	D207R	GCCTTGTGGGTCCTTCTTG CG CGCCCA AAAGTAGTCAC
M352R_Q356R_ K360Es	Forward	M352R/Q35 6R/K360E	GCG GAAGACCCAGC GG CTGGAGAT CG AGTTGAGCAACAAGACCGAGGAGG
M352R_Q356R_ K360Eas	Reverse	M352R/Q35 6R/K360E	CT CG ATCTCCAGC CG CTGGGTCTT CCG CTCCAGGTCTTTCTGCCGCTCTG
K370E_R374Es	Forward	K370E/R37 4E	GGACATC G AGAAGGCACGG G AGAAGT CCTCAGGCCGGAGATG
K370E_R374Eas	Reverse	K370E/R37 4E	GCCTGAGTGGACTT TC CCGTGCCTTC T CG ATGTCCTCCTCGGTC
K396Es	Forward	K396E	CAACCAGGCCCAGTCC G AGTGGTTTGA AGAGATG
K396Eas	Reverse	K396E	CATCTCTTCAAACCACT CG GACTGGGC CTGGTTG
I359C-Forward	Forward	I359C	GAAGACCCAGCAGCTGGAG TG CAAGT TGAGCAACAAGAC
I359C-Reverse	Reverse	I359C	GTCTTGTTGCTCAACTTG CA CTCCAGCT GCTGGGTCTTC
F398C-Forward	Forward	F398C	GGCCCAGTCCAAGTGGT GT GAAGAGA TGGTGACGACC
F398C-Reverse	Reverse	F398C	GGTCGTCACCATCTCTT CA ACCACTT GGACTGGGC
H431C-Forward	Forward	H431C	CAGTACACACAGCTGCGG TG CGAGAC GGACATGTTC
H431C-Reverse	Reverse	H431C	GAACATGTCCGTCTCG CA CCGCAGCTG TGTGTACTG
G213C-Forward	Forward	G213C	CAAGAAGGACCCACA A TGCAATGGCA CGGTGG
G213C-Reverse	Reverse	G213C	CCACCGTGCCATTGC A TTGTGGGTCCT TCTTG
D207C-Forward	Forward	D207C	CTGTGACTACTTTTGGGCG TG CAAGAA GGACCCACAAG
D207C-Reverse	Reverse	D207C	CTTGTGGGTCCTTCTTG CA CGCCAAA AGTAGTCACAG
R326C-Forward	Forward	R326C	CACCACATCGCTGACCT TG CAAGCAG CTGGCGAGCCGC

R326C-Reverse	Reverse	R326C	GCGGCTCGCCAGCTGCTT GCA GAGGTC AGCGATGTGGTG
W397C-Forward	Forward	W397C	GGCCCAGTCCAAGTG CTTT GAAGAGAT GGTG
W397C-Reverse	Reverse	W397C	CACCATCTCTTCAA AG CACTTGGACTG GGCC

Table 2: List of constructed plasmids.

No	Plasmid	Purpose
1	pGEX6P1 EGFP GAS7c	For <i>in vitro</i> assay
2	pGEX6P1 GFP GAS7b	For <i>in vitro</i> assay and fluorescence microscopy
3	pGEX6P1 EGFP GAS7 F-BAR	For <i>in vitro</i> assay
4	pGEX6P1 GFP CIP4 F-BAR	As positive control
5	pGEX6P1 EGFP C1	For <i>in vivo</i> assay
6	pEGFP GAS7b Δ E171-E197 (Δ FFL1)	For <i>in vivo</i> assay
7	pEGFP GAS7b N177P	For <i>in vivo</i> assay
8	pEGFP GAS7b D207R	For <i>in vivo</i> assay
9	pEGFP GAS7b K209E	For <i>in vivo</i> assay
10	pEGFP GAS7b Δ K209-T216 (Δ FFL2)	For <i>in vivo</i> assay
11	pEGFP GAS7b Q212R	For <i>in vivo</i> assay
12	pEGFP GAS7b E221A	For <i>in vivo</i> assay
13	pEGFP GAS7b R242E	For <i>in vivo</i> assay
14	pEGFP GAS7b D319A	For <i>in vivo</i> assay
15	pEGFP GAS7b R326A	For <i>in vivo</i> assay
16	pEGFP GAS7b R326D	For <i>in vivo</i> assay
17	pEGFP GAS7b K327A	For <i>in vivo</i> assay
18	pEGFP GAS7b K327D	For <i>in vivo</i> assay
19	pEGFP GAS7b E351A	For <i>in vivo</i> assay
20	pEGFP GAS7b M352R/Q356R/K360E	For <i>in vivo</i> assay
21	pEGFP GAS7b K370E/R374E	For <i>in vivo</i> assay
22	pEGFP GAS7b K396E	For <i>in vivo</i> assay
23	pEGFP GAS7b W397S	For <i>in vivo</i> assay
24	pEGFP GAS7b H431A/M435A	For <i>in vivo</i> assay

25	pEGFP GAS7b Q438A	For <i>in vivo</i> assay
26	pEGFP GAS7b R449A	For <i>in vivo</i> assay
27	pEGFP GAS7b W460S	For <i>in vivo</i> assay
28	pEGFP GAS7 F-BAR ΔE171-E197 (ΔFFL1)	For <i>in vivo</i> assay
29	pEGFP GAS7 F-BAR N177P	For <i>in vivo</i> assay
30	pEGFP GAS7 F-BAR D207R	For <i>in vivo</i> assay
31	pEGFP GAS7 F-BAR K209E	For <i>in vivo</i> assay
32	pEGFP GAS7 F-BAR ΔK209-T216 (ΔFFL2)	For <i>in vivo</i> assay
33	pEGFP GAS7 F-BAR Q212R	For <i>in vivo</i> assay
34	pEGFP GAS7 F-BAR E221A	For <i>in vivo</i> assay
35	pEGFP GAS7 F-BAR R242E	For <i>in vivo</i> assay
36	pEGFP GAS7 F-BAR D319A	For <i>in vivo</i> assay
37	pEGFP GAS7 F-BAR R326A	For <i>in vivo</i> assay
38	pEGFP GAS7 F-BAR R326D	For <i>in vivo</i> assay
39	pEGFP GAS7 F-BAR K327A	For <i>in vivo</i> assay
40	pEGFP GAS7 F-BAR K327D	For <i>in vivo</i> assay
41	pEGFP GAS7 F-BAR E351A	For <i>in vivo</i> assay
42	pEGFP GAS7 F-BAR M352R/Q356R/K360E	For <i>in vivo</i> assay
43	pEGFP GAS7 F-BAR K370E/R374E	For <i>in vivo</i> assay
44	pEGFP GAS7 F-BAR K396E	For <i>in vivo</i> assay
45	pEGFP GAS7 F-BAR W397S	For <i>in vivo</i> assay
46	pEGFP GAS7 F-BAR H431A/M435A	For <i>in vivo</i> assay
47	pEGFP GAS7 F-BAR Q438A	For <i>in vivo</i> assay
48	pEGFP GAS7 F-BAR R449A	For <i>in vivo</i> assay
49	pEGFP GAS7 F-BAR W460S	For <i>in vivo</i> assay
50	pGEX6P1 GAS7c	For TEM
51	pGEX6P1 GAS7b	For TEM and cryo-TEM
52	pGEX6P1 GAS7 F-BAR	For TEM
53	pGEX6P1 GAS7b ΔE171-E197 (ΔFFL1)	Non-tagged for <i>in vitro</i> assay
54	pGEX6P1 GAS7b N177P	Non-tagged for <i>in vitro</i> assay
55	pGEX6P1 GAS7b D207R	Non-tagged for <i>in vitro</i> assay
56	pGEX6P1 GAS7b ΔK209-T216 (ΔFFL2)	Non-tagged for <i>in vitro</i> assay
57	pGEX6P1 GAS7b Q212R	Non-tagged for <i>in vitro</i> assay

58	pGEX6P1 GAS7b R326A	Non-tagged for <i>in vitro</i> assay and cryo-TEM
59	pGEX6P1 GAS7b K370E/R374E	Non-tagged for <i>in vitro</i> assay
60	pGEX6P1 GAS7 F-BAR ΔE171-E197 (ΔFFL1)	Non-tagged for <i>in vitro</i> assay
61	pGEX6P1 GAS7 F-BAR N177P	Non-tagged for <i>in vitro</i> assay
62	pGEX6P1 GAS7 F-BAR D207R	Non-tagged for <i>in vitro</i> assay
63	pGEX6P1 GAS7 F-BAR ΔK209-T216 (ΔFFL2)	Non-tagged for <i>in vitro</i> assay
64	pGEX6P1 GAS7 F-BAR Q212R	Non-tagged for <i>in vitro</i> assay
65	pGEX6P1 GAS7 F-BAR R326A	Non-tagged for <i>in vitro</i> assay
66	pGEX6P1 GAS7 F-BAR K370E/R374E	Non-tagged for <i>in vitro</i> assay
67	pGEX6P1 GFP GAS7b ΔE171-E197 (ΔFFL1)	GFP-tagged for <i>in vitro</i> assay
68	pGEX6P1 GFP GAS7b N177P	GFP-tagged for <i>in vitro</i> assay
69	pGEX6P1 GFP GAS7b D207R	GFP-tagged for <i>in vitro</i> assay
70	pGEX6P1 GFP GAS7b ΔK209-T216 (ΔFFL2)	GFP-tagged for <i>in vitro</i> assay
71	pGEX6P1 GFP GAS7b Q212R	GFP-tagged for <i>in vitro</i> assay
72	pGEX6P1 GFP GAS7b R326A	GFP-tagged for <i>in vitro</i> assay
73	pGEX6P1 GFP GAS7b K370E/R374E	GFP-tagged for <i>in vitro</i> assay
74	pGEX6P1 EGFP GAS7 F-BAR ΔE171-E197 (ΔFFL1)	GFP-tagged for <i>in vitro</i> assay
75	pGEX6P1 GFP GAS7 F-BAR N177P	GFP-tagged for <i>in vitro</i> assay
76	pGEX6P1 GFP GAS7 F-BAR D207R	GFP-tagged for <i>in vitro</i> assay
77	pGEX6P1 EGFP GAS7 F-BAR ΔK209-T216 (ΔFFL2)	GFP-tagged for <i>in vitro</i> assay
78	pGEX6P1 EGFP GAS7 F-BAR Q212R	GFP-tagged for <i>in vitro</i> assay
79	pGEX6P1 EGFP GAS7 F-BAR R326A	GFP-tagged for <i>in vitro</i> assay
80	pGEX6P1 EGFP GAS7 F-BAR K370E/R374E	GFP-tagged for <i>in vitro</i> assay

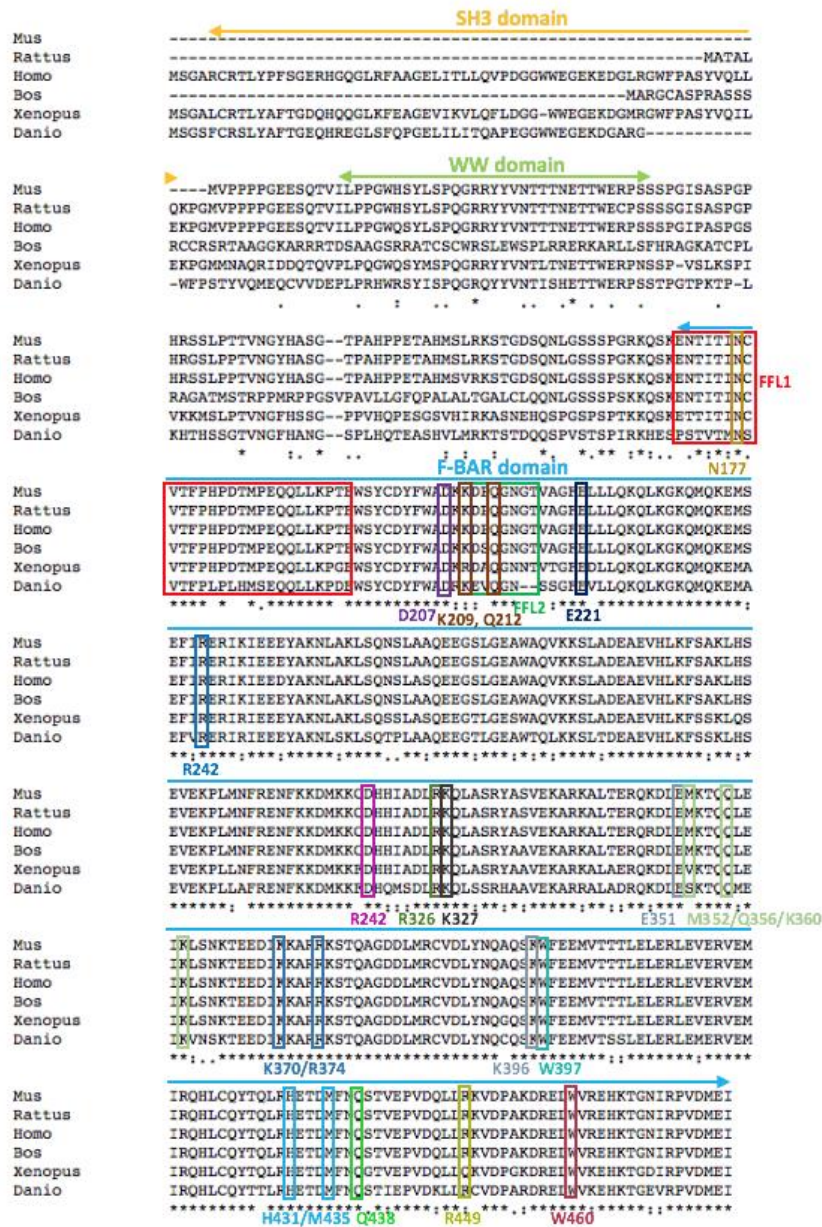


Figure 12: GAS7 splicing isoforms and structure-based alignment of the F-BAR domain sequences. The alignment was compared between Mus (mouse), Rattus (rat), Homo (human), Bos (cattle), Xenopus (frog), and Danio (zebrafish) sequences.

2.5 Cell cultures

GAS7b, GAS7 F-BAR and their mutations; Δ FFL1 (171-197 aa deletion), Δ FFL2 (206-219 aa deletion), K370E/R374E, Q212R, R326A, N177P, and D207R mutant were cloned into a pEGFP-C1 vector, and EGFP was substituted with its brighter variant, Venus. DsRed-membrane was expressed using a pDsRed-monomer-Mem vector (Clontech). HeLa cells were cultured in DMEM supplemented with 10% FBS as described previously. Transfection was performed with Lipofectamine LTX and PLUS reagents (Invitrogen) according to the

manufacturer's instructions. The cells were observed with a confocal microscope (Olympus FV1000D).

2.6 Liposome preparations and liposome co-sedimentation assay

The liposome binding assay was performed as follows. Liposomes were made from total bovine brain lipids (Folch Fraction 1, Avanti), which the fraction rich in phosphatidylserine (PS). 0.2% of Rhodamine-PE was incorporated to facilitate visualization of the liposome fraction. The lipids were dissolved in chloroform in a glass tube, mixed and dried under N₂ gas to produce a thin, homogenous lipid film. The residual chloroform from the film was removed by placing the glass tube in a vacuum desiccator, for a minimum of 20 min. The dried lipid was re-suspended in buffer containing 200 mM NaCl or 300 mM NaCl, 10 mM Tris-HCl pH 7.5, 1 mM EDTA and the tube was sealed and incubated at 37°C for 1-2 h to form liposomes. The tubes were vortexed after the incubation. The proteins (0.5 μM and 2.3 μM) and liposomes (0.4 μg/μl) were mixed and were incubated at room temperature for 20 min. After incubation, the liposomes were precipitated by centrifugation at 50,000 rpm, for 20 min at 25°C, using TLA100 rotor (Beckman Coulter). The supernatant and pellet were supplemented with 8 μl of the 5 x SDS-PAGE sample buffer, and then examined by SDS-polyacrylamide gel electrophoresis (SDS-PAGE), and visualized by CBB staining. Figure 13 shows the illustration on liposome co-sedimentation assay. EGFP-CIP4 F-BAR was used as positive control.

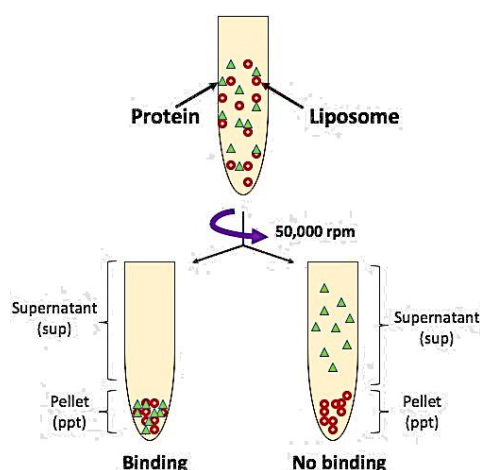


Figure 13: Liposome co-sedimentation assay.

2.7 Preparation of PC:PS:PE-GUVs

Giant vesicles were prepared by natural swelling as follows. Phosphatidylcholine (PC, P3841), phosphatidylserine (PS, P5660) and phosphatidylethanolamine (PE, P7693) were purchased

from Sigma-Aldrich. PC:PS:PE-GUVs were prepared according to Alam Shibly *et al.* (2016), with slight modifications. The GUVs were prepared by natural swelling in water (MiliQ), containing 300 mM sucrose. To make GUV with 1.0 mM PC, 1.0 mM of PE and 3.0 mM of PS, these lipids were prepared in chloroform, in a glass tube and then chloroform was evaporated by N₂ gas to produce thin, homogenous lipid film. The residual chloroform in the film was removed by placing the glass tube in a vacuum desiccator connected to a pump for >25 min. Twenty µl of buffer containing 10 mM of Tris-HCl (pH 7.5), 300 mM sucrose and 1.0 mM EDTA added into the glass tube and the glass tube was sealed and incubated at 45 °C for 8 min (prehydration). 230 µl of the same buffer was added, and the tube was resealed and incubated in an incubator at 37 °C for 2 hr to produce a GUV suspension.

2.8 Fluorescence microscopy

After the incubation, the GUV was observed under IX70 (Olympus) fluorescence microscope, mixing together with 1% BSA as blocking buffer. To observe the protein binding on GUVs, 0.5 µM of protein was added with the same amount of volume as the GUVs and was incubated at room temperature for 20 min before observation.

2.9 Transmission electron microscopy

Ten µl of liposomes (0.4 µg/µl) were incubated both in the absence and presence of 10 µl of protein (0.5 and 2.3 µM) for 20 min at 30°C. The resulting sample of 20 µl was applied to formvar-coated copper grid (Nisshin EM) and incubated for 1 min. Excess liquid was carefully removed by using Whatman filter paper. The grid was then incubated for few seconds with 100 mM HEPES (pH 7.5). Excess liquid was again removed carefully with Whatman filter paper. The grid was incubated with 0.5% uranyl acetate solution for 1 min and was dried on the filter paper. Liposome morphologies were examined on Hitachi H-7100 Transmission Electron Microscope (TEM), with electron energy set to 75 kV. Representative images were taken on an AMT camera with a direct magnification of 2k × - 12k ×.

2.10 Cryo-transmission electron microscopy

Giant vesicles were prepared as mentioned above. After incubation, the tag-cleaved GAS7b (0.5 µM) and giant vesicles were then incubated for 5 min at room temperature. The mixture was placed on a glow discharged molybdenic electron microscopy grid coated with holey carbon film (Quantifoil R1.2/1.3, Mo 200 mesh). After blotting the excess liquid with the tip of filter

papers, the sample was embedded in vitreous ice by plunge-freezing into liquid ethane using an FEI rapid-freezing apparatus (FEI Vitrobot). The vitrified specimen was transferred to an advanced cryo-electron microscope (FEI Titan Krios) operated at 300 kV acceleration voltage and equipped with an image corrector, a direct electron detector (Falcon II, FEI), and a Volta phase plate. Images were recorded with a nominal magnification of 29,000 (pixel size of 2.37 Å on the specimen) under the low-dose condition (total electron dose: ~ 12 electrons/Å²).

2.11 Crosslinking assays

The crosslinking assay was performed by utilizing the following procedure. Two types of crosslinker reagents were used, BS(PEG)5 and Sulfo-EGS [ethylene glycolbis(sulfosuccinimidylsuccinate)] (Thermo Scientific), with different spacer arm length of 21.4 Å and 16.1 Å, respectively. DMSO was used to dissolve BS (PEG)5, while HEPES-containing buffer was used to dissolve Sulfo EGS reagents, to a final stock concentration of 1 mM. Proteins (1.0 μM) of 12 μl, which were purified in a buffer that does not contain any primary amines, were mixed with 12 μl of crosslinker reagents at different concentrations and incubated at room temperature for 30 min. The stock of the crosslinker reagents were diluted with HEPES-containing buffer, and was added to the proteins to obtain final concentrations of 0.01 mM, 0.02 mM, 0.04 mM and 0.06 mM of crosslinker reagents, with the final concentration of 0.5 μM proteins. The final concentration of DMSO in the BS(PEG)5 reagent added to the proteins was 3%. The HEPES-containing buffer consisted of 0.01 mM HEPES at pH 8.0, 150 mM NaCl, 1 mM EDTA. The reaction was quenched by adding Tris buffer to a final concentration of 25 mM Tris, for 15 min at room temperature. Both DMSO and buffer were used as negative controls. The reaction was examined by western blot, using mouse anti-GAS7 (2F6, Origene) as the primary antibody.

As for the crosslinking assays in the presence of liposome, the following procedure was done. Proteins (2.0 μM) of 48 μl, which were purified in a buffer that does not contain any primary amines, were mixed with 48 μl of bovine brain Folch (0.4 μg/μl) and incubated at room temperature for 20 min. Then, 22 μl of this protein and liposome mixture were mixed with 22 μl of crosslinker reagents at different concentrations and incubated at room temperature for 30 min. The final concentrations of the crosslinker reagents used were 0.02 mM, 0.04 mM and 0.06 mM, with the final concentration of 0.5 μM proteins. The final concentration of DMSO in the BS(PEG)5 reagent added to the proteins was 3%. The reaction was quenched by adding Tris buffer to a final concentration of 25 mM Tris, for 15 min at room temperature. Both DMSO

and buffer were used as negative controls. The reaction was examined by western blot, using mouse anti-GAS7 (2F6, Origene) as the primary antibody.

2.12 Statistical analyses

All data are expressed as the mean \pm s.d., as indicated in the legends. The data for each condition were obtained from at least three independent experiments. The statistical analyses were performed with Microsoft Excel, using the Student's t-test. A value of $P < 0.05$ was considered significant.

3.0 Results

3.1 Binding activity of GAS7 isoforms to the liposomes

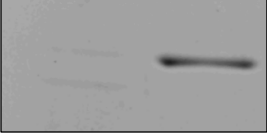
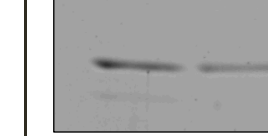
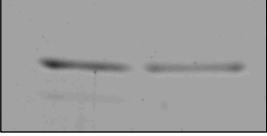

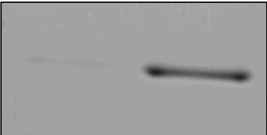
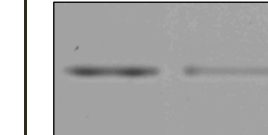
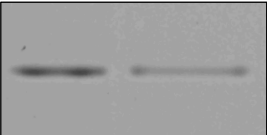

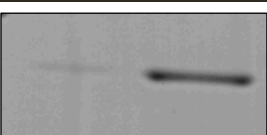
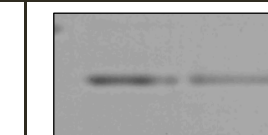
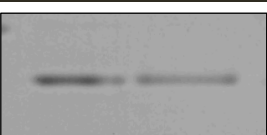

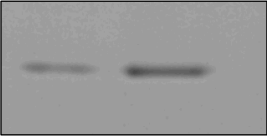

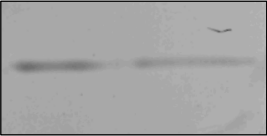

3.1.1 Liposome co-sedimentation assay

In order to examine the binding ability of GAS7 proteins to liposome, I examined the binding of all GAS7 isoforms; GAS7c, GAS7b and GAS7 F-BAR (as shown in Figure 9) to liposomes made of bovine brain Folch fraction. The effect of membrane binding for this protein is to form curvature on the membrane. The bovine brain Folch used in this study are rich in phosphatidylserine (PS, 46 %), phosphatidylcholine (PC, 17%), phosphatidylethanolamine (PE, 9%), phosphatidylinositol (PI, 8%), and small amounts of phosphatidylinositol phosphates (PIPs) and phosphatidylinositol (4, 5)-bisphosphate (PI (4, 5) P₂) (Michelsen *et al.*, 1995). The Folch fraction lipids are usually used because they contain all kinds of lipids in the brain, and the BAR domain studies was started with the interest in synaptic vesicles recycling. The Folch fraction is rich in phosphatidylserine, a negatively charged phospholipids, and thus, the liposomes are negatively charged.

After incubation of the liposome with protein, then the proteins bound to liposomes were separated by ultra-centrifugation, and then the supernatant and the pellet were resolved by SDS-PAGE. The percentage of proteins that bound to liposomes were calculated from the percentage of precipitated proteins with the liposomes among the total proteins. The precipitation of the liposome was confirmed by the visualization of lipids in both the supernatants and precipitates by the rhodamine-labelled PE that was incorporated to 0.2% during the liposome preparation.

The liposome binding was examined in two salt conditions; the normal salt concentration (200 mM) and the high salt concentration (300 mM). The high salt concentration was used to observe the effect of salt on the membrane binding, which is supposed to weaken the electrostatic interactions. I used CIP4 F-BAR as the positive control. Figure 14 shows the representative images of SDS-PAGE for each isoform (Figure 14a) and the quantification of the proteins in the pellet (Figure 14b), under the normal salt concentration. Figure 15 shows the representative images of SDS-PAGE (Figure 15a) and the quantification of the proteins in pellet (Figure 15b), under high salt concentration. All GAS7 isoforms showed high binding ability towards liposomes (>80%) in the normal salt conditions (Figure 14b). However, in the high salt conditions, the binding of GAS7 isoforms decreased (Figure 15b).

a.

Proteins	Normal salt concentration (200 mM)			
	+ Liposome		- Liposome	
	sup	pt	sup	pt
GAS7c				
GAS7b				
GAS7 F-BAR				
CIP4 F-BAR				

b.

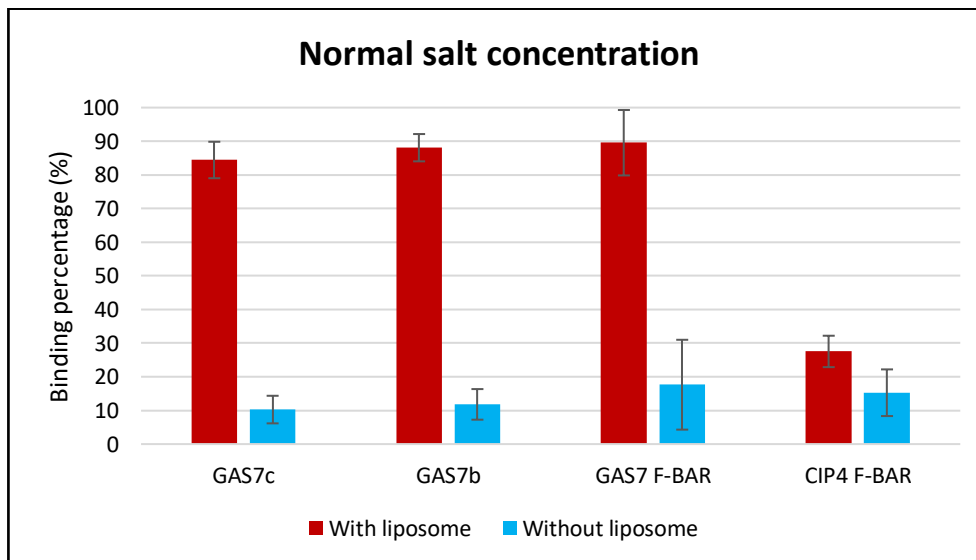
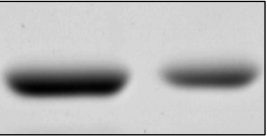
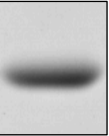
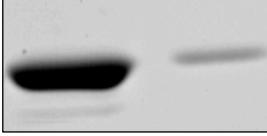

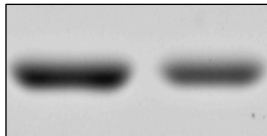
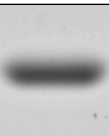
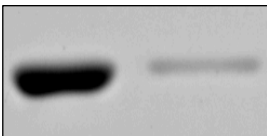
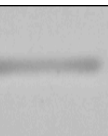
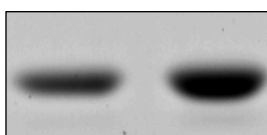
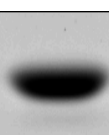
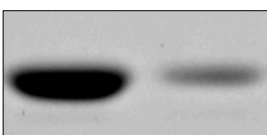
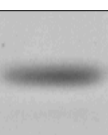
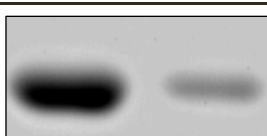
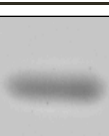
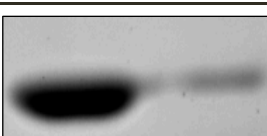
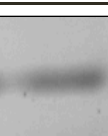


Figure 14: Liposome co-sedimentation assay. GFP-GAS7 isoforms (GAS7c, GAS7b, and GAS7 F-BAR) and CIP4 F-BAR as positive control (2.3 μ M) were examined for their binding to liposome composed of total bovine brain lipid at normal salt concentration (200 mM). (a) Representative of the SDS-PAGE images from the assay. The presence of proteins in pellet (pt) indicates membrane binding. (b) Quantification of proteins in pellet from Figure 14a with liposomes. Sup: supernatant. N=3. Error bars: SD. The P-values were obtained by two-tailed Student's t-test. All isoforms are significant, $p < 0.01$, against the positive control.

a.

Proteins	High salt concentration (300 mM)			
	+ Liposome		- Liposome	
	sup	pt	sup	pt
GAS7c				
GAS7b				
GAS7 F-BAR				
CIP4 F-BAR				

b.

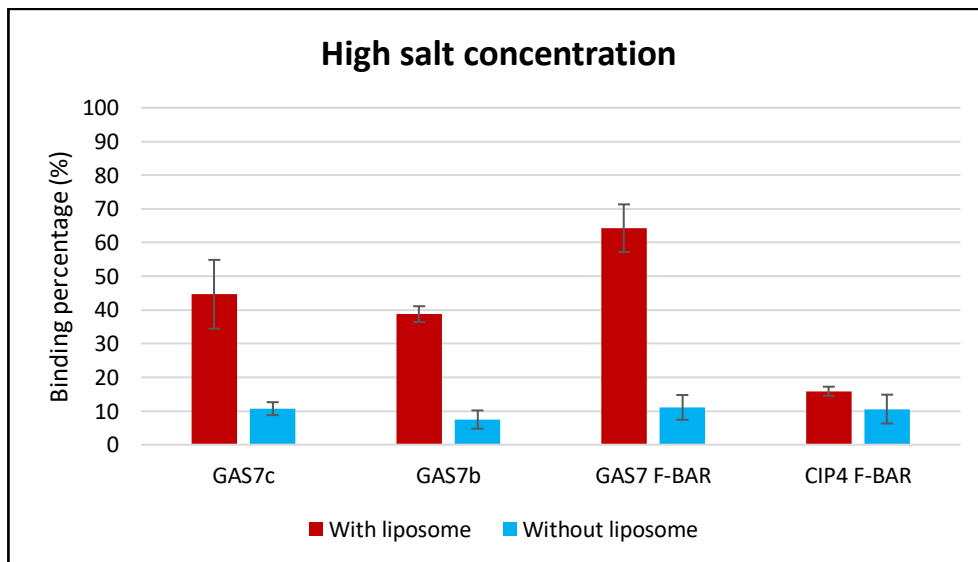


Figure 15: Liposome co-sedimentation assay. GFP-GAS7 isoforms (GAS7c, GAS7b, and GAS7 F-BAR) and CIP4 F-BAR as positive control (2.3 μ M) were examined for their binding to liposome composed of total bovine brain lipid at high salt concentration (300 mM). (a) Representative of the SDS-PAGE images from the assay. The presence of proteins in pellet (pt) indicates membrane binding. (b) Quantification of proteins in pellet from Figure 15a with liposomes. Sup: supernatant. N=3. Error bars: SD. The P-values were obtained by two-tailed Student's t-test. All isoforms are significant, $p < 0.01$, against the positive control.

The co-sedimentation assay revealed that all three isoforms have the ability to bind to liposomes, both in the normal and the high salt concentrations. Since the Folch fraction is rich in phosphatidylserine, a negatively charged phospholipids, and thus, the liposomes are negatively charged. Therefore, GAS7 and the liposomes are thought to bind through the electrostatic interactions, providing the mutants to be analyzed and the reason behind the decreased in binding in high salt concentrations.

3.1.2 Transmission electron microscopy

In order to support our data from the liposome co-sedimentation assay, I examined the morphology of the Folch liposome incubated with each GAS7 isoforms, using transmission electron microscope (TEM). These liposomes have typically diameters of maximum several micro-meters. Proteins that binds to the membrane, were able to formed tubulations on liposomes (Inaba *et al.*, 2016). I observed the liposomes under TEM with the magnification 12, 000x. I found that all GAS7 isoforms formed tubules, but some liposomes remained without tubules. Tubules were form in all isoforms, in both salt concentrations (Figure 16). This observation supports our liposome co-sedimentation assay data in the previous section.

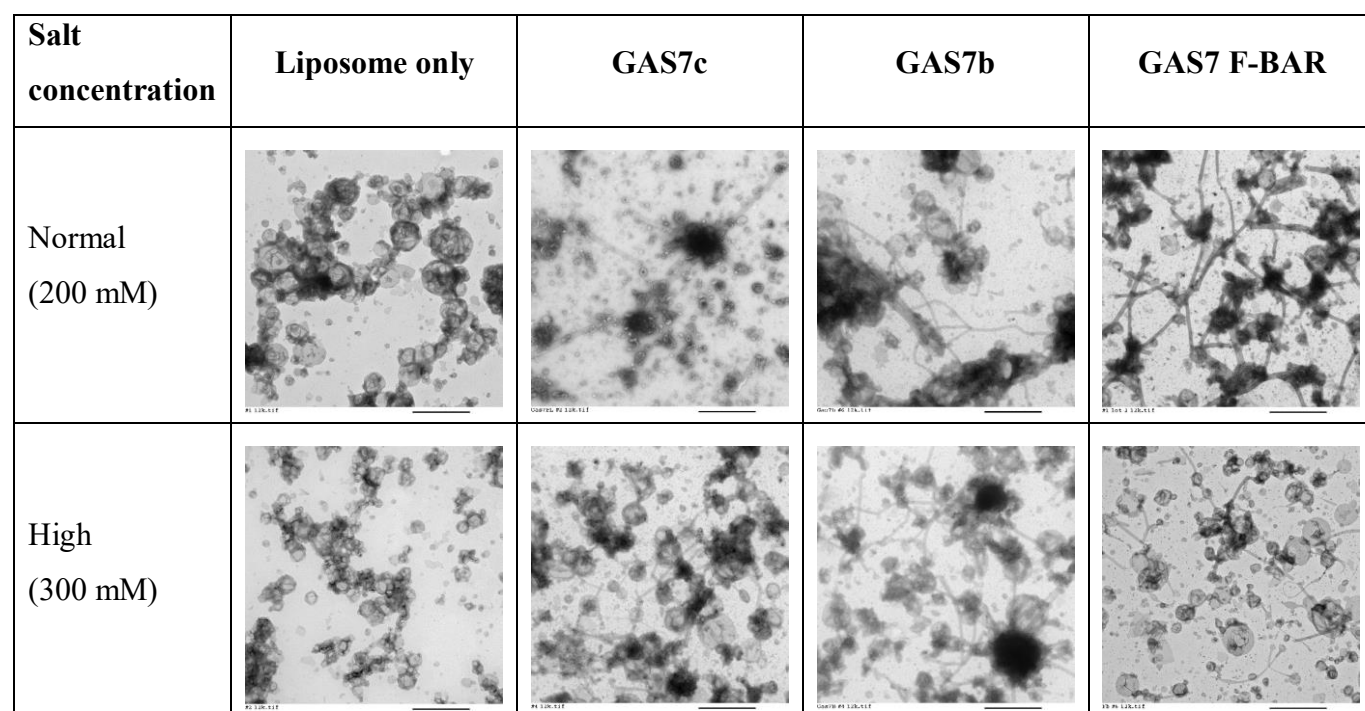


Figure 16: Representative images of GAS7 isoforms through transmission electron microscopy. GAS7 isoforms (2.3 μ M) were examined for their binding to liposome composed of total bovine brain Folch at normal (200 mM) and high (300 mM) salt concentration. N=3. Magnification 12, 000x. Scale bar: 2 μ m.

3.1.3 GAS7b on the GUV

3.1.3.1 GFP-GAS7b on GUV

I examined the binding and localization of GAS7b on giant unilamellar vesicles (GUV), which have diameters of several-ten micro-meters. The GUV composition was PS: PC: PE=3:1:1, in 200 mM salt condition. Using fluorescence microscopy, there was no fluorescence signal detected in GUV only (Figure 17). However, in the presence of GFP-GAS7b, a GFP-fluorescence protein was detected surrounding on the surface of the GUVs. The GAS7b assembled into the patch on the GUV, without forming prominent tubules from GUV. This showed that GAS7b binds and assembles on the membrane.

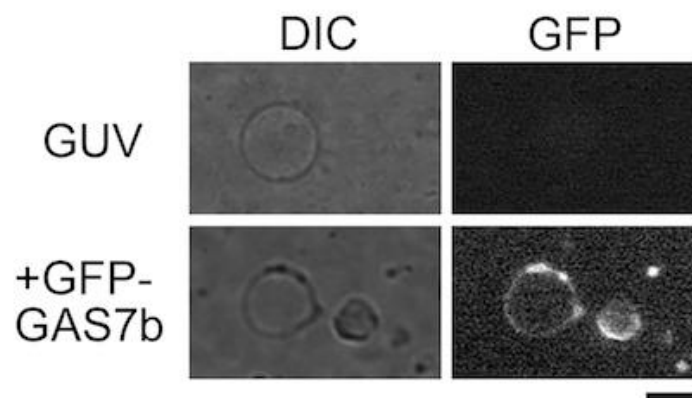


Figure 17: Fluorescence microscopy images showing the binding of GAS7b on the membrane of GUV. The image on the top side is the GUV without the protein. Bottom images show the binding of GAS7b on GUV membrane. Scale bar: 50 μm .

3.1.3.2 Cryo-transmission electron microscopy (cryo-EM) on GAS7b

I examined the binding and localization of GAS7 on the giant unilamellar vesicles (GUV) incubated using untagged-GAS7b, using phase contrast cryo-electron microscopy (cryo-EM), which has enhanced contrast in focus. I specifically focused on GAS7b as GAS7b was reported to bind to N-WASP, which are involved with actin polymerization and to be involved in actin cytoskeleton for various cellular phenomenon (You *et al.*, 2010; Tseng *et al.*, 2015). As compared to the protein-free liposomes, the liposome with $\sim 1 \mu\text{m}$ in diameter with GAS7b had striations. The striations indicate that there were binding between the proteins and the liposomes. Sometimes, the striations on the liposomes had a spacing of $\sim 19 \text{ nm}$ in one and $\sim 6 \text{ nm}$ in the second dimension (Figure 18b). These values were comparable to those of the FFOs in the crystal, suggesting that GAS7 forms FFOs on membranes. Cryo-EM images in Figure 18a (right) shows the binding of GAS7b on GUV.

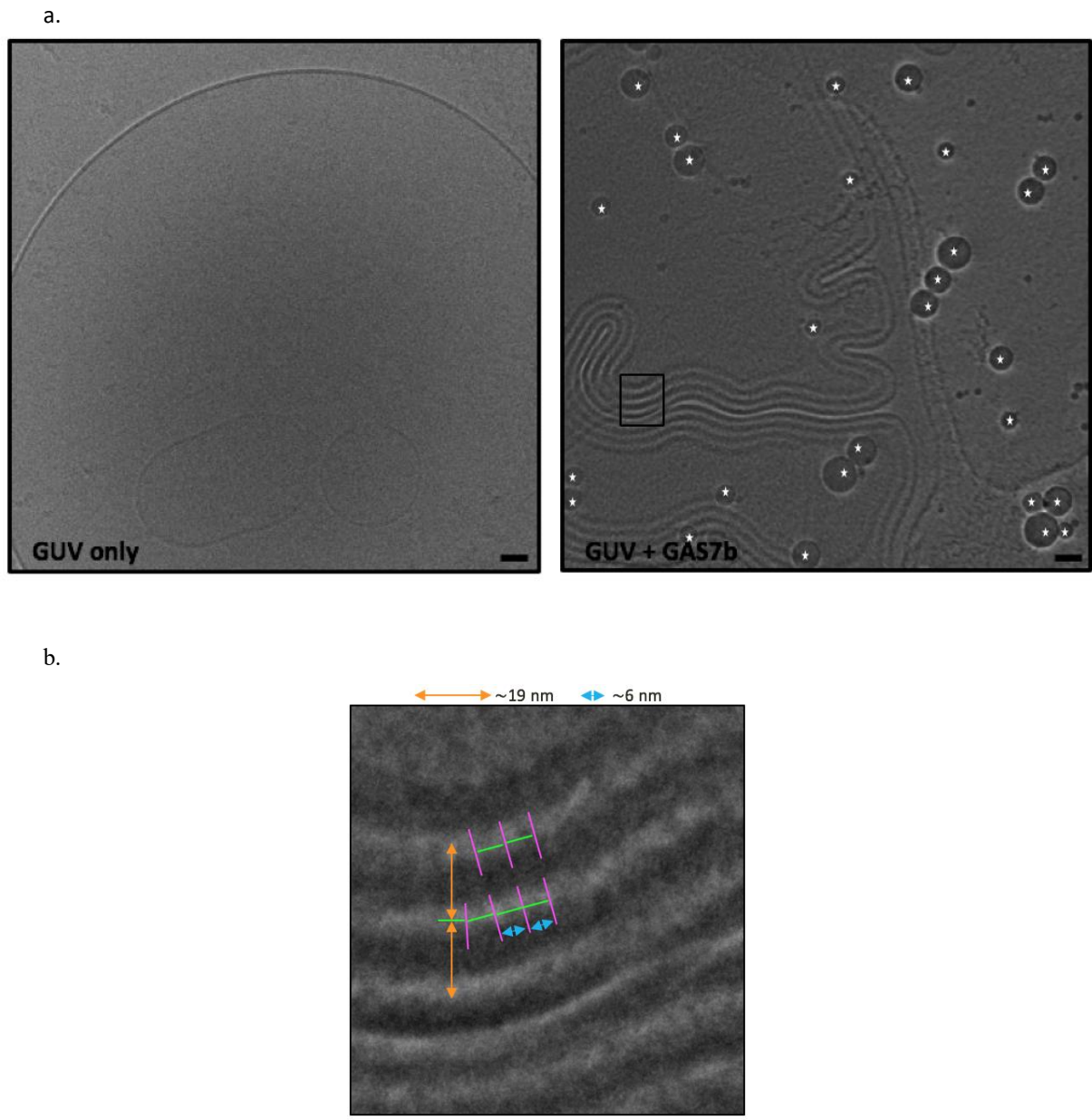


Figure 18: Cryo-EM images showing the binding of GAS7b on the membrane of GUV. (a) The image on the left is the GUV without the protein. Right image shows the binding of GAS7b on GUV membrane. Striations can be observed on the right image, suggesting there is a binding between GAS7b protein and GUV. Asterisks (*) indicate ice crystal contaminations. Scale bar: 100 nm. (b) The enlarged image of the region indicated by a black rectangle in (a). Scale bar: 20 nm.

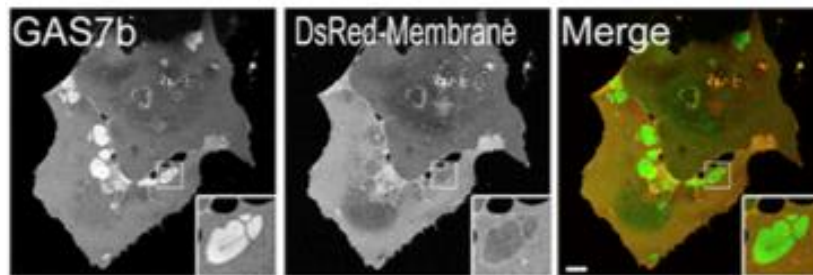
3.2 Mutations on GAS7 F-BAR domain

Based on our data, I have found that all GAS7 isoforms were able to bind to the membrane, and assemble on the membrane. However, the mechanisms of membrane binding of GAS7 and of the assembly of GAS7 were unclear. Hence, to discover the binding mechanism, we decided to introduce mutations on the F-BAR domain that were thought to play role in the binding ability to the membrane.

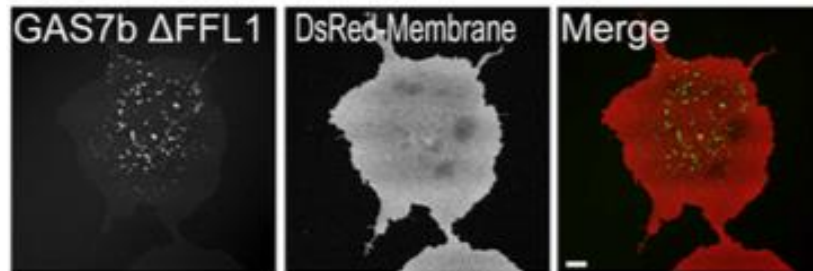
3.2.1 Mutations of the GAS7 loops

The GAS7 F-BAR protein structure consists of two loops, known as the filament forming loop 1 (FFL1; aa 171-197) and filament forming loop 2 (FFL2; aa 206-219) (as shown in Figure 8a). Based on the GAS7 F-BAR crystal structure, both of these FFLs were hypothesized to be involved with the FFO formation. To determine the roles of both FFL1 and FFL2 for the membrane binding of GAS7, I made the mutants with deletion of FFLs. Firstly, I expressed the mutants in HeLa cells. In HeLa cells, the assembly of GAS7 was examined with GFP tag and the membrane was visualized by the palmitoylated DsRed-monomer (DsRed-membrane), a diffusive plasma membrane marker. In GAS7b wild type (WT), the patches of several microns were formed, which excluded the DsRed membrane. This suggest that the patches are protein assembly like sheets composed of highly concentrated GAS7b (Figure 19a). Then, I expressed the GAS7b Δ FFL1 and GAS7b Δ FFL2 mutants in HeLa cells (Figure 19b and 19c). Both of these mutants showed a significantly reduced patches formation, as compared to GAS7b WT. This suggested that FFL1 and FFL2 were involved in the patch formation in the HeLa cells.

a.



b.



c.

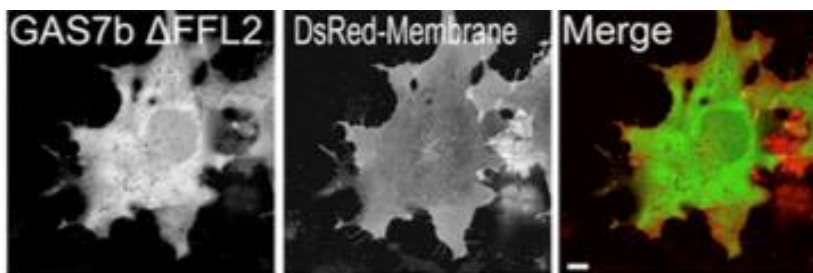
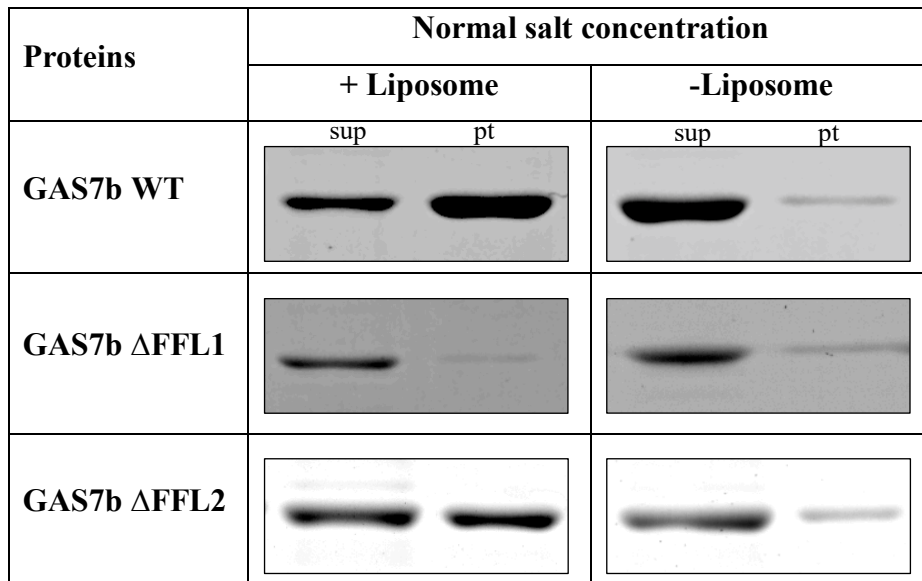


Figure 19: Expression of GFP-GAS7b (a) and its mutation, Δ FFL1 (b) and Δ FFL2 (c), on HeLa cells, visualized by confocal microscopy. The plasma membranes of the cells were visualized by co-expression of DsRed-membrane. Scale bars: 10 μ m. The enlarged images of the regions indicated by squares are shown at the bottom right for GAS7b WT (a).

To examine the correlation of cellular membrane localization of the GAS7 to the *in vitro* membrane binding, I performed the *in vitro* membrane-binding assay, that I utilized the liposome co-sedimentation assay. Representative images of the gel from this assay are shown in Figure 20a. This assay revealed that the binding of both GAS7b Δ FFL1 and GAS7b Δ FFL2 mutants on liposomes were significantly reduced, compared to that of GAS7b WT (Figure 20b). Therefore, the cellular membrane localization of GAS7 was consistent with the membrane binding *in vivo and in vitro*, proving that these loops played significant roles in the membrane binding. Because FFL1 and FFL2 were at the contact sites between dimers in the crystals, the same configuration of the dimers was suggested to occur in the cells.

a.



b.

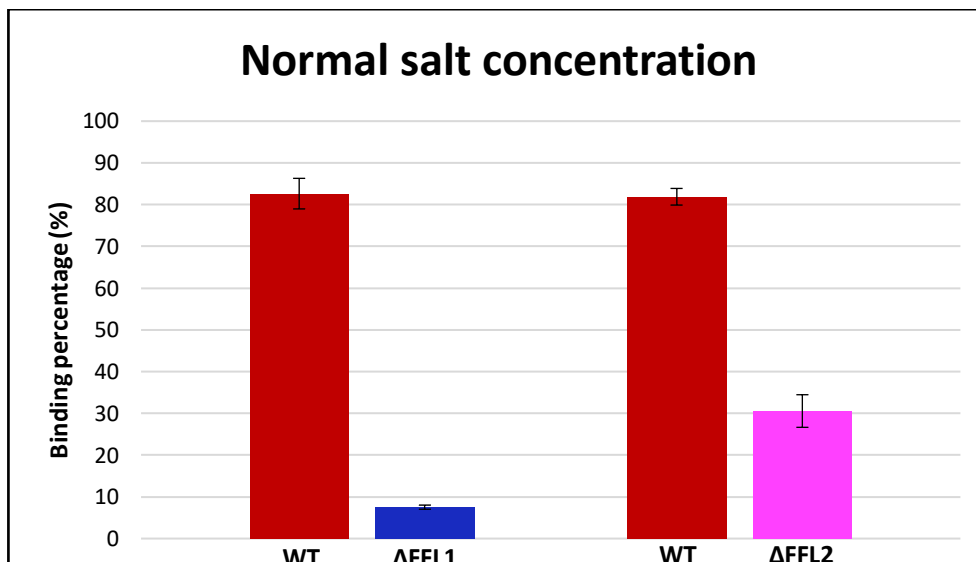


Figure 20: Liposome co-sedimentation assay. GFP-GAS7b WT and its mutations, Δ FFL1 and Δ FFL2 (0.5 μ M) were examined for their binding to liposome composed of total bovine brain lipid at normal salt concentration (200 mM). (a) Representative of the SDS-PAGE images from the assay. The presence of proteins in pellet (pt) indicates membrane binding. (b) Quantification of proteins in pellet from Figure 20a with liposomes. Sup: supernatant. N=3. Error bars: SD. The P-values were obtained by two-tailed Student's t-test. All isoforms are significant, $p < 0.01$, against the positive control.

To examine the electrostatic interactions between the membrane and GAS7b and possibly between GAS7s on the assembly, I examined the binding of these mutants at high salt concentration of 300 mM NaCl (Figure 21). As the salt concentration increased, the binding between GAS7b WT and liposomes was decreased, as compared in normal salt concentration (Figure 20b). The binding of GAS7b Δ FFL2 mutants was decreased as compared to GAS7b

WT (Figure 21b). However, I could not quantify the proteins in pellet for Δ FFL1, due to protein degradation at high salt concentration. The binding of GAS7b Δ FFL2 was decreased to $\sim 1/3$, while the binding of GAS7 decreased to $\sim 1/2$ as compared to those binding in normal salt concentration (Figure 20b). Therefore, FFL2 was suggested to contribute to the assembly through electrostatic interactions.

a.

Proteins	High salt concentration			
	+ Liposome		-Liposome	
	sup	pt	sup	pt
GAS7b WT				
GAS7b ΔFFL2				

b.

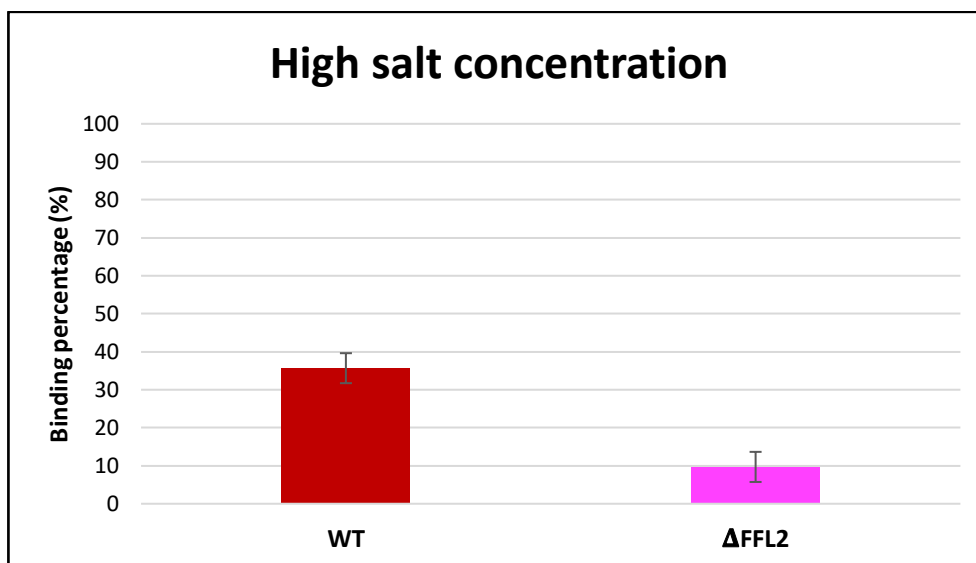
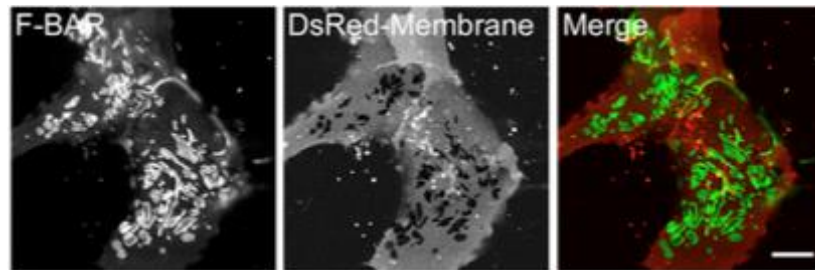


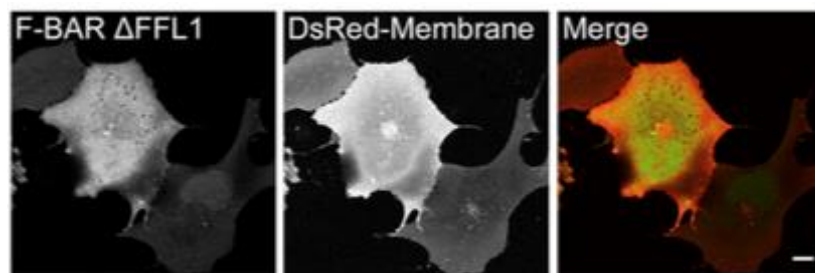
Figure 21: Liposome co-sedimentation assay. GFP-GAS7b WT and its mutations Δ FFL2 (0.5 μ M) were examined for their binding to liposome composed of total bovine brain lipid at high salt concentration (300 mM). (a) Representative of the SDS-PAGE images from the assay. The presence of proteins in pellet (pt) indicates membrane binding. (b) Quantification of proteins in pellet from Figure 21a with liposomes. Sup: supernatant. N=3. Error bars: SD. The P-values were obtained by two-tailed Student's t-test. All isoforms are significant, $p < 0.01$, against the positive control.

The *in vivo* experiment was also performed using GAS7 F-BAR. GAS7 F-BAR WT showed patches (Figure 22a) when it was expressed on HeLa cells, the same as in GAS7b WT (Figure 19a). Then, I expressed the GAS7 F-BAR Δ FFL1 and GAS7 F-BAR Δ FFL2 mutants in HeLa cells. Both mutants abolished patch formation, as compared to GAS7 F-BAR WT (Figure 22b and 22c).

a.



b.



c.

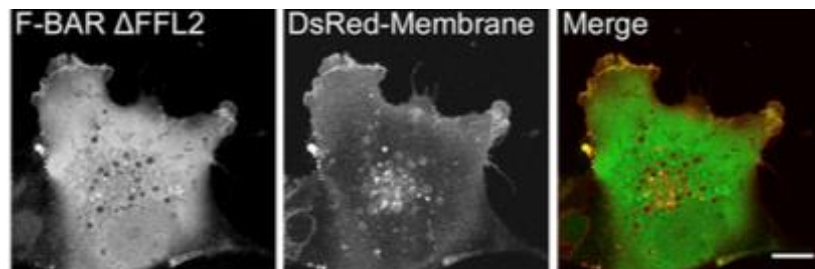


Figure 22: Expression of GFP-GAS7F-BAR WT(a) and its mutation, Δ FFL1 (b) and Δ FFL2 (c), on HeLa cells, visualized by confocal microscopy. The plasma membranes of the cells were visualized by co-expression of DsRed-membrane. Scale bars: 10 μ m. The enlarged images of the regions indicated by squares are shown at the bottom right for GAS7 F-BAR WT (a).

All these data suggested that the interactions between GAS7 dimers through both FFL1 and FFL2 were essential for membrane interaction. Based on the F-BAR domain crystal structure, one of the two FFL1s (Figure 23, blue) at the convex surface of the dimer interacts with the tip of the adjacent dimer. The deletion of FFL1 will affect the protein oligomerization on the membrane surface, reducing the binding between the proteins and the membrane.

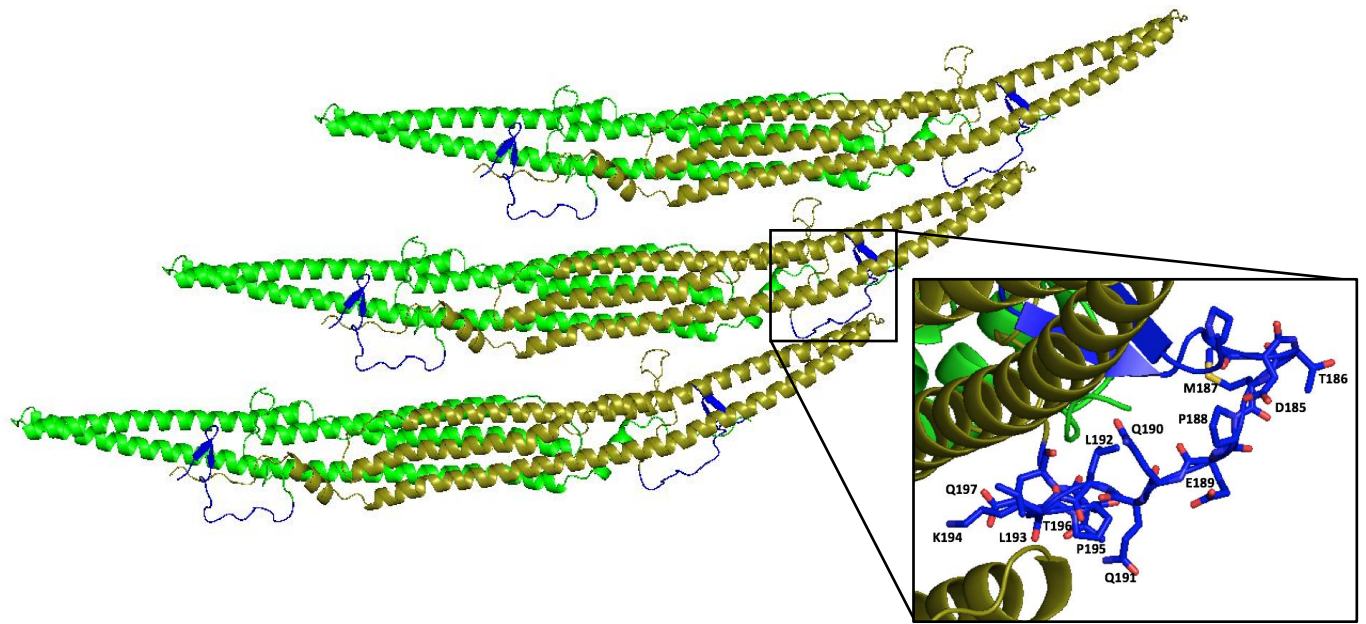


Figure 23: Ribbon diagrams of GAS7 F-BAR crystal structure, showing FFL1 locations (blue). Insert: One of the two FFL1 interacts with the tip of adjacent dimer. This close-up view showing the sidechains of FFL1 that interacts with the adjacent dimers.

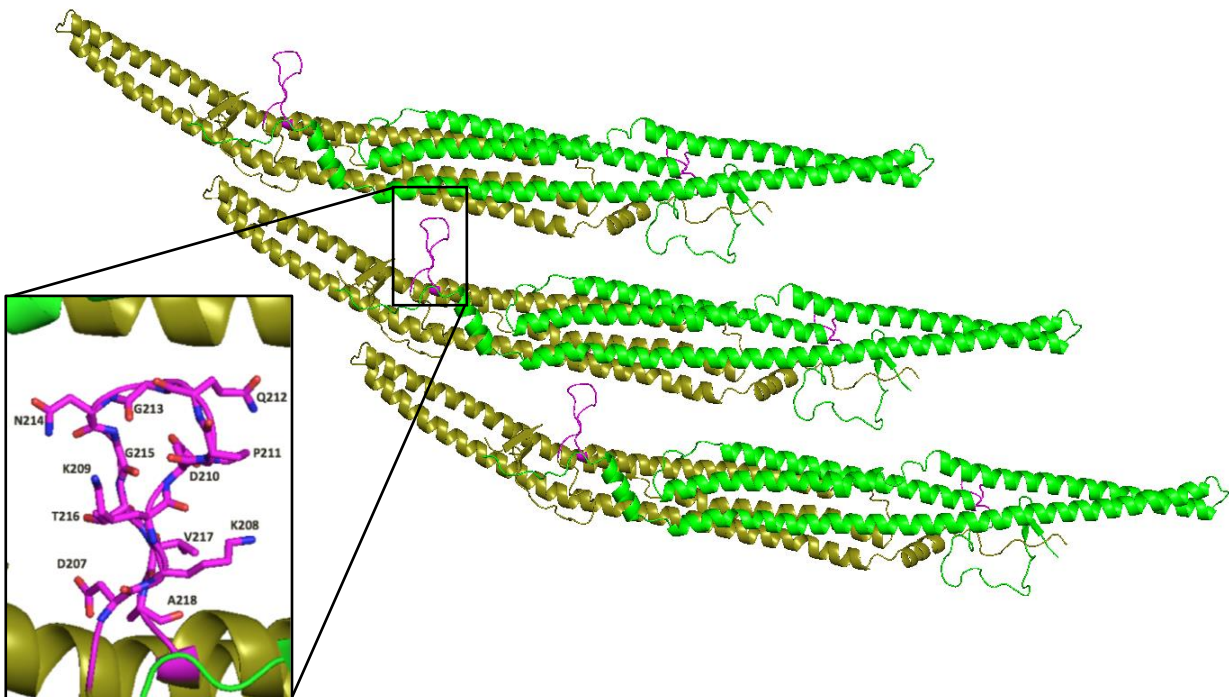


Figure 24: Ribbon diagrams of GAS7 F-BAR crystal structure, showing FFL2 locations (magenta). Insert: One of the two FFL2 interacts with the tip of adjacent dimer. This close-up view showing the sidechains of FFL2 that interacts with the adjacent dimers.

As for FFL2, one of the two FFL2s at the convex surface of the dimer interacts with a conserved region on the convex surface of the adjacent dimer in the FFO (Figure 24, magenta).

The deletion of this FFL2 is thought to affect the oligomerization. When the assembly of these oligomers is hindered by the deletions, the formation of the protein oligomers on the membrane surface will also be inhibited, resulting in the reduced membrane binding activity.

One of the FFL2 of the F-BAR dimer, have no contact with the adjacent dimer in the FFO. We presumed that this surface of free FFL2 as the surface that interacts with membrane surface.

3.2.2 FFL2 without protein contact interacts with membrane surface

The crystal structure of GAS7 F-BAR domains showed that one of the FFL2 of the F-BAR

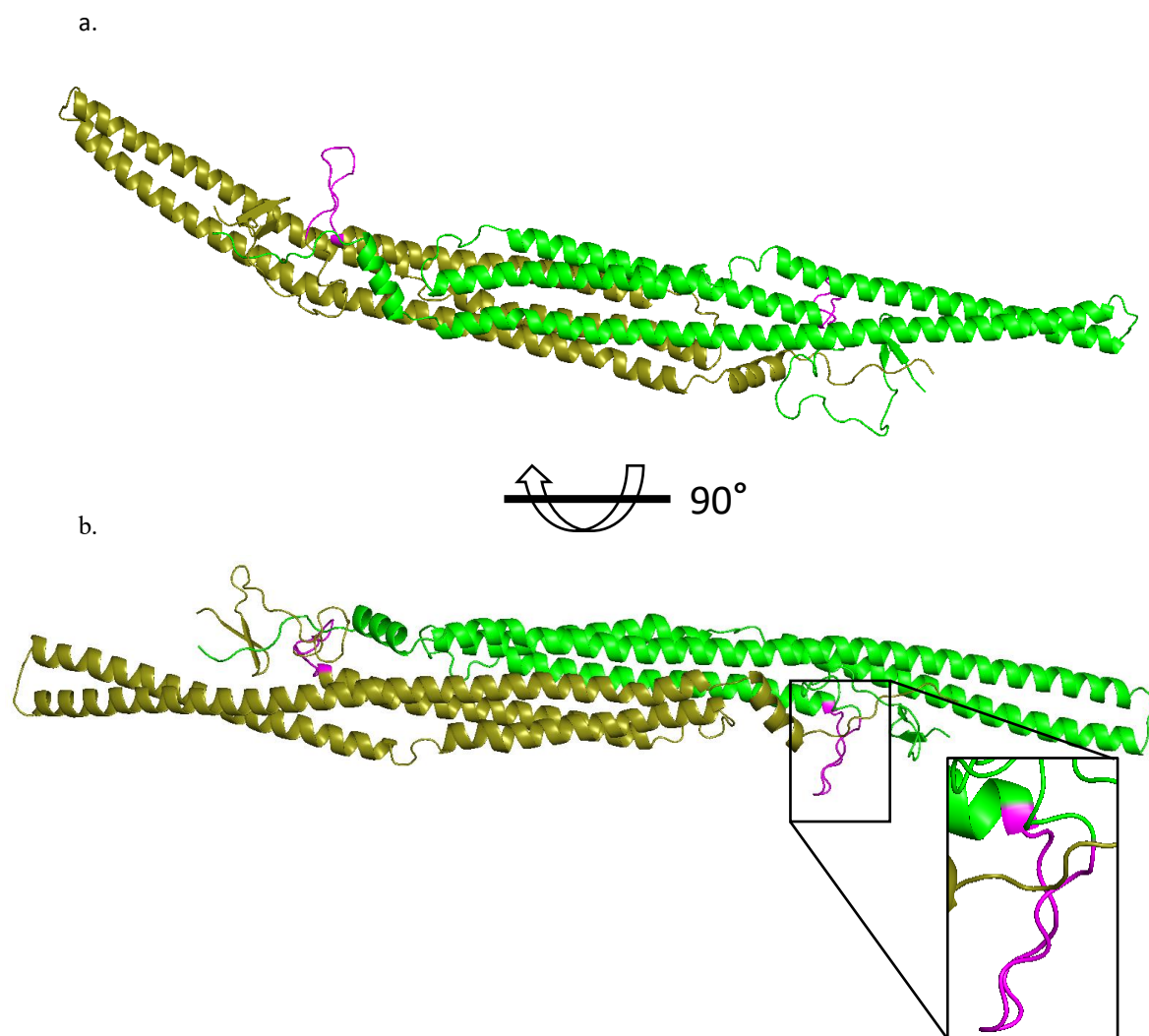
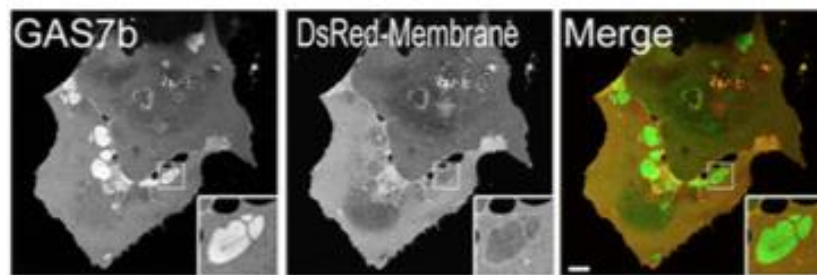


Figure 25: Ribbon diagrams of GAS7 F-BAR crystal structure, showing FFL2 locations (magenta). (a) One of the two FFL2 interacts with the tip of adjacent dimer, as shown in Figure 24. (b) Another FFL2 which does not interact with any adjacent dimers (insert). Q212 is shown in skyblue. Therefore, the two FFL2s were placed perpendicular each other.

dimer, has no contact with the adjacent dimer (Figure 25b, insert). This FFL2 was exposed to the solvent. Thus, I decided to replace Glutamine 212, which was located at the tip of the FFL2, with Arginine (Q212R). Arginine (Arg), a positively charge amino acids, was expected to strengthened the binding between the liposome, which is negatively charge, with the proteins.

Interestingly, The Q212R mutant, with substitution of uncharged to positively charged amino-acid residue, formed patches, which is similar to the GAS7b WT (Figure 26).

a.



b.

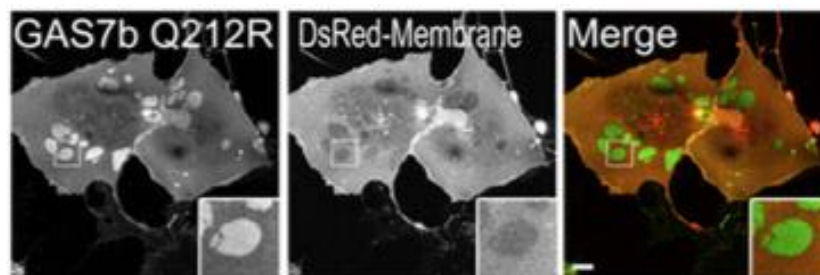
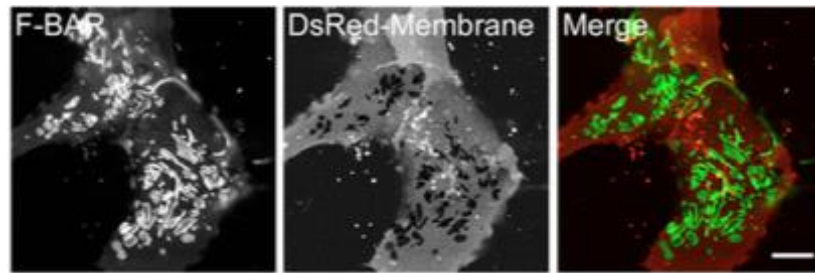


Figure 26: Expression of GFP-GAS7b WT (a) and its mutation, Q212R (b), on HeLa cells, visualized by confocal microscopy. The plasma membranes of the cells were visualized by co-expression of DsRed-membrane. Scale bars: 10 μ m. The enlarged images of the regions indicated by squares are shown at the bottom right for GAS7b WT (a) and GAS7b Q212R (b).

I also found the patches were formed on HeLa cells, infected with GAS7 F-BAR Q212R (Figure 27). The patches formation on this mutation was similar to GAS7 F-BAR WT.

a.



b.

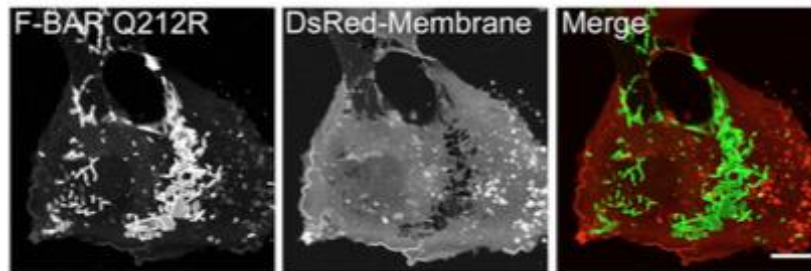


Figure 27: Expression of GFP-GAS7 F-BAR WT (a) and its mutation, Q212R (b), on HeLa cells, visualized by confocal microscopy. The plasma membranes of the cells were visualized by co-expression of DsRed-membrane. Scale bars: 10 μm . The enlarged images of the regions indicated by squares are shown at the bottom right for GAS7 F-BAR WT (a) and GAS7 F-BAR Q212R (b).

I performed liposome co-sedimentation assay for GAS7b Q212R mutants, in both normal and high salt conditions (Figure 28), to examine the binding of this mutation on membrane.

a.

Proteins	Normal salt concentration		High salt concentration	
	+ Liposome	-Liposome	+ Liposome	-Liposome
GAS7b WT	sup pt	sup pt	sup pt	sup pt
GAS7b Q212R	sup pt	sup pt	sup pt	sup pt

b.

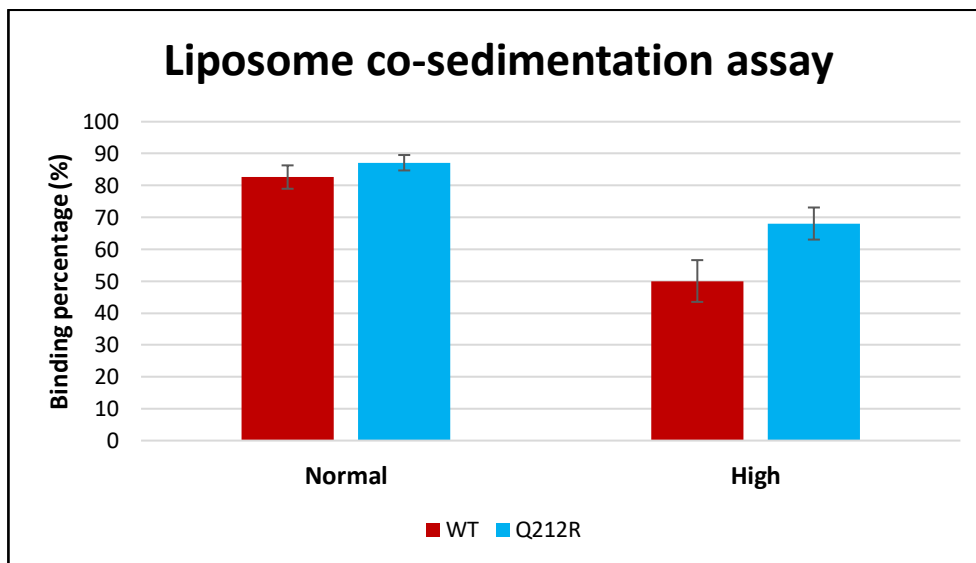


Figure 28: Liposome co-sedimentation assay. GFP-GAS7b WT and its mutation, Q212R (0.5 μ M) were examined for their binding to liposome composed of total bovine brain lipid at normal (200 mM) and high salt concentration (300 mM). (a) Representative of the SDS-PAGE images from the assay. The presence of proteins in pellet (pt) indicates membrane binding. (b) Quantification of proteins in pellet from Figure 28a with liposomes. Sup: supernatant. N=3. Error bars: SD. The P-values were obtained by two-tailed Student's t-test. All isoforms are significant, $p < 0.01$, against the positive control.

Q212R was shown to have stronger binding under both salt concentrations, as compared to GAS7b WT. These results indicated that one of the two FFL2 were exposed to the membrane surface. Therefore, FFL2 was not likely to be involved in membrane insertion, in contrast with the “wedge loop” of PACSIN2 F-BAR domains; which is hydrophobic. The surface of FFL2 without interaction with the adjacent GAS7 F-BAR dimer could be involved in the membrane binding.

3.2.3 The point mutants of the membrane binding surface and the dimer-dimer interaction (oligomerization)

The next question raised from this F-BAR domain crystal structure is that how does the oligomerization of GAS7 works on the membrane. To answer this question, I introduced 19 mutations on the F-BAR domain at the contact sites between the dimers in the crystal. All these mutations were selected based on their contacts to the adjacent dimers in the crystal, which might affect the oligomerization between dimers. All of these mutations point were mutated by changing their amino acid side chain group; uncharged and charged polar group to non-polar group, non-polar group to charged or uncharged polar group, positively charged group to negatively charged group vice versa, and uncharged to charged polar group. These mutants include N177P, D207R, K209E, E221A, R242E, D319A, R326A, R326D, K327A, K327D, E351A, M352R/Q356R/K360E, K396E, W397S, H431A/M435A, Q438A, R449A, and W460S.

There are several amino-acid residues that were suggested to contact with the membrane, as Q212. We made the K370E/R374E mutant, where the mutated residues were on the same surface as the Q212 at FFL2 without contact to the adjacent GAS7.

All the 19 mutations are shown in Figure 29, and their suggested roles are summarized in Table 3.

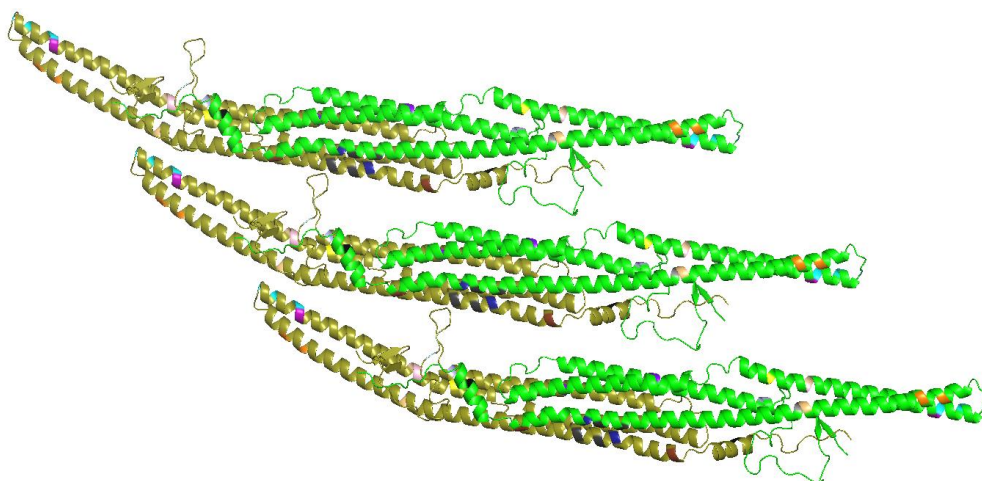


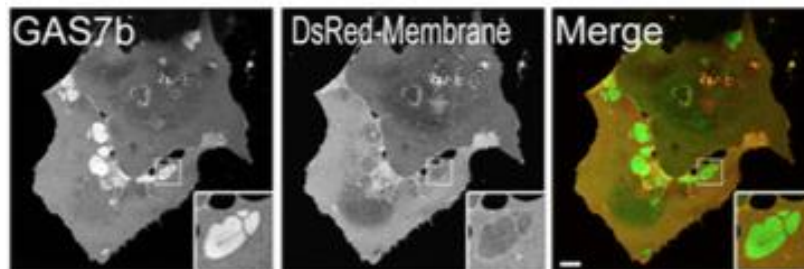
Figure 29: Ribbon diagram of the GAS7 F-BAR domain crystal structure, with 19 introduced mutations. The amino acids that were introduced with mutations are N177 (sand), D207 (palecyan), K209 (smudge), E221 (lightblue), R242 (purpleblue), D319 (yellow), R326 (lightpink), K327 (wheat), E351 (purple), M352/Q356/K360 (cyan), K370/R374 (orange), K396 (lightorange), W397 (gray60), H431/M435 (gray20), Q438 (density), R449 (chocolate), and W460 (black).

Table 3: Suggested functions for each point of mutations.

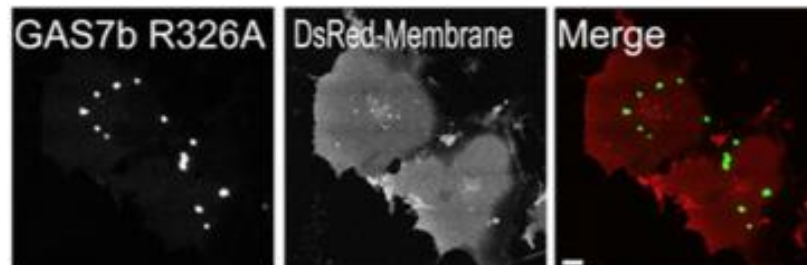
Suggested functions of mutation point	Point of mutation
Contact surface within dimers	N177, D207, K209, E221, R242, D319, R326, K327, E351, M352/Q356/K360, K396, W397, H431/M435, Q438, R449 and W460
Contact surface with membrane	Q212, K370/R374

The membrane localization of all these 19 mutants were examined using HeLa cells. Two mutants were shown to exhibit a significant reduction in the patch formation, as compared to GAS7b WT. These mutations were R326A and K370E/R374E (Figure 30).

a.



b.



c.

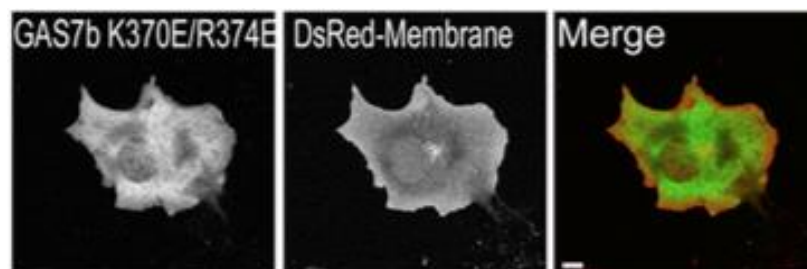


Figure 30: Expression of GAS7b WT (a) and its mutations, R326A (b), and K370E/R374E (c) on HeLa cells, visualized by confocal microscopy. The plasma membranes of the cells were visualized by co-expression of DsRed-membrane. Scale bars: 10 μ m. The enlarged images of the regions indicated by squares are shown at the bottom right for GAS7b WT (a).

R326 has contacts with N177 of FFL1 and D207 of FFL2, and thus R326 is supposed to contribute to the stability of the FFLs (Figure 31). K370/R374 are exposed to solvent, and thus are thought to contact with the membrane (Figure 32). Hence, I named R326A mutation as the stabilizing mutant and K370E/R374E as the surface interaction mutant.

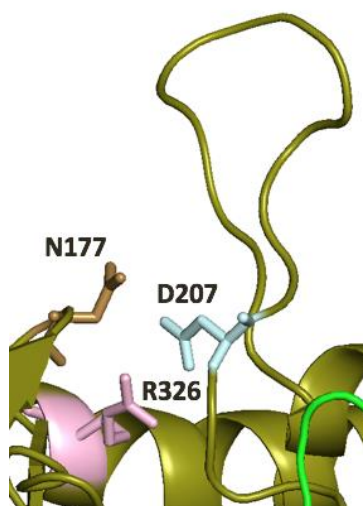


Figure 31: Ribbon diagram of GAS7 F-BAR domain crystal structure showing the contact sites between R326 (lightpink), N177 (sand) and D207 (palecyan). FFL1 is represented by blue and FFL2 is represented by magenta. The amino acid that was mutated are shown in stick.

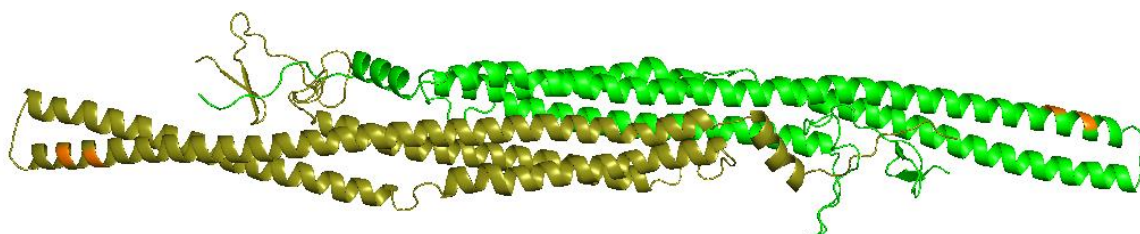


Figure 32: Ribbon diagram of GAS7 F-BAR domain crystal structure showing the contact sites between K370/R374 (orange) with the membrane surface.

3.2.4 The mutants that affect the stability of FFLs

R326 has contacts with N177 on FFL1 and D207 on FFL2. Figure 29 and Figure 31 show that R326 was found to interact with these both FFLs. The average distance between each mutant were as follows; N177 and D207 was 3.3 Å, N177 and R326 was 3.1 Å and D207 and R326 was 2.7 Å in the crystal (Figure 33).

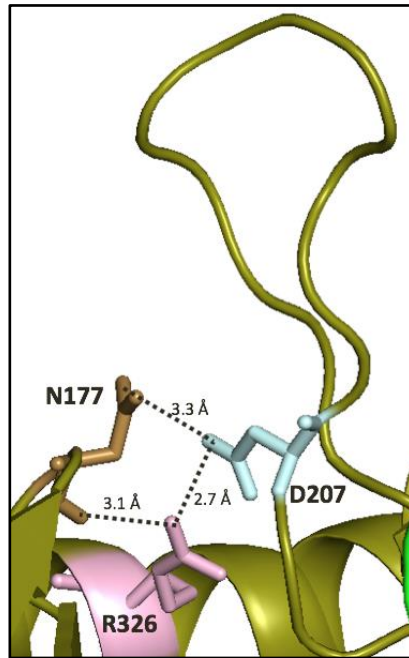


Figure 33: Ribbon diagram of GAS7 F-BAR domain crystal structure showing the contact sites between R326 (lightpink), N177 (sand) and D207 (palecyan). The average distance between N177 and D207 was 3.3 Å, N177 and R326 was 3.1 Å and D207 and R326 was 2.7 Å.

I investigated the membrane binding of N177P and D207R mutants expressed as GFP fusion protein by liposome co-sedimentation assay, in both normal and high salt concentrations. Representative images of the SDS-PAGE from this assay are shown in Figure 34(a) and its quantification is shown in Figure 34(b) for both normal and high salt concentrations. As for the R326A mutants, I couldn't express this mutant in GFP-tagged samples as protein degradation occurs, hence, I performed this mutation on a non-tagged GAS7b samples.

a.

Proteins (GFP-tagged)	Normal salt concentration		High salt concentration	
	+ Liposome	-Liposome	+ Liposome	-Liposome
	sup pt	sup pt	sup pt	sup pt
GAS7b WT				
GAS7b N177P (FFL1)				
GAS7b D207R (FFL2)				

b.

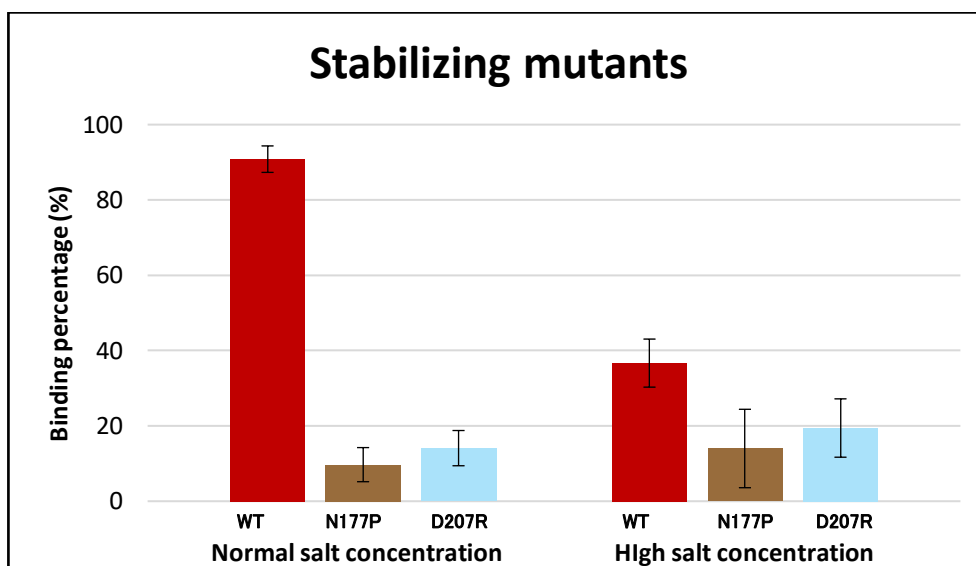


Figure 34: Liposome co-sedimentation assay, for stabilizing mutants. GFP-GAS7b WT and its mutation, N177P and D207R (0.5 μ M) were examined for their binding to liposome composed of total bovine brain lipid at normal (200 mM) and high salt concentration (300 mM). (a) Representative of the SDS-PAGE images from the assay. The presence of proteins in pellet (pt) indicates membrane binding. (b) Quantification of proteins in pellet from Figure 34a with liposomes. Sup: supernatant. N=3. Error bars: SD. The P-values were obtained by two-tailed Student's t-test. All isoforms are significant, $p < 0.01$, against the positive control.

N177P and D207R showed a decrease in binding in both salt concentrations. Therefore, these two amino-acid residues could be important in stabilization of the FFLs for oligomer formation. When I tested the membrane binding of non-tagged GAS7b WT and these mutants, there was a significant decreased in the binding between R326A and the liposomes in the

normal salt concentration. However, there was no significant decreased in the high salt concentration (Figure 35). This data probably represented the binding surface of the other part of FFL2. It shows that this surface was partly mediated by direct binding of R326 to the membrane. This proved that R326A plays an important role for protein oligomerization, but not in membrane surface interaction.

I couldn't examine the binding of non-tagged GAS7b N177P and non-tagged GAS7b D207R mutants as protein degradations occurred during the protein purification steps, causing multiple bands to appear on the SDS PAGE images. Therefore, R326A mutant could have retained some membrane binding ability. I concluded that, the oligomer formation and the membrane binding is closely related but could be separable phenomena when the FFLs were not deleted.

a.

Proteins	Normal salt concentration		High salt concentration	
	+ Liposome	-Liposome	+ Liposome	-Liposome
GAS7b WT	sup pt	sup pt	sup pt	sup pt
GAS7b R326A	sup pt	sup pt	sup pt	sup pt

b.

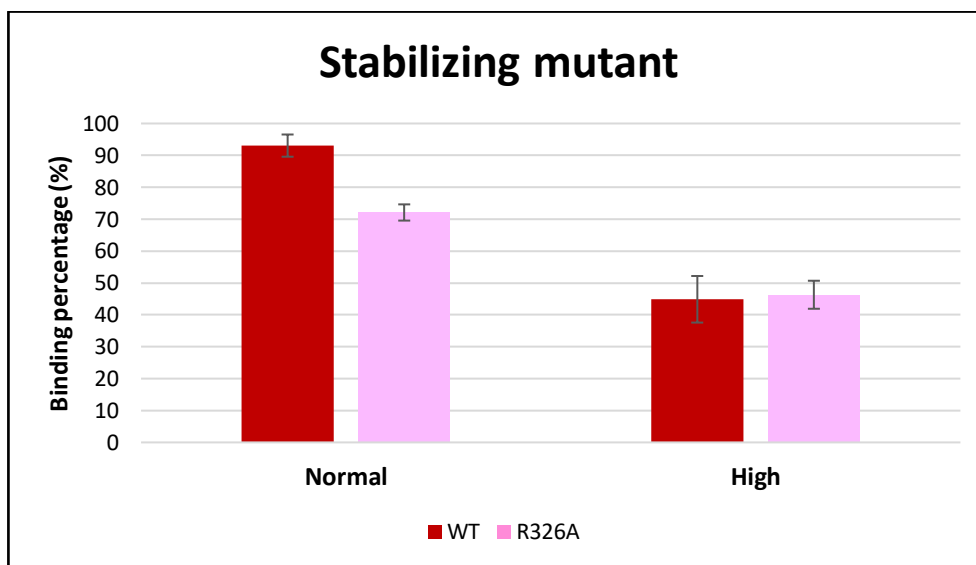


Figure 35: Liposome co-sedimentation assay, for stabilizing mutant. Non-tagged GAS7b WT and its mutation, R326A (0.5 μ M) were examined for their binding to liposome composed of total bovine brain lipid at normal (200 mM) and high salt concentration (300 mM). (a) Representative of the SDS-PAGE images from the assay. The presence of proteins in pellet (pt) indicates membrane binding. (b) Quantification of proteins in pellet from Figure 35a with liposomes. Sup: supernatant. N=3. Error bars: SD. The P-values were obtained by two-tailed Student's t-test. All isoforms are significant, $p < 0.01$, against the positive control.

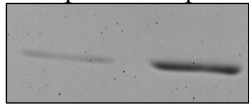
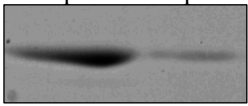
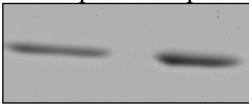
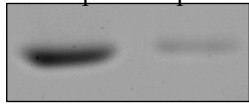
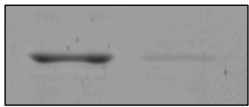
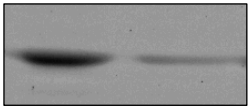
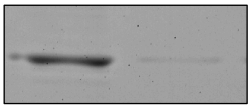
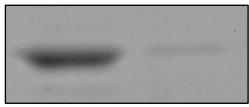
3.2.5 Surface interaction mutant

K370/R374, which is located at the FFO surface, was suggested to have contact sites with the membrane surface (as shown in Figure 32). The *in vivo* assay as shown in Figure 30(c) shows reduction of patches in HeLa cells. When I tested this mutation for its ability to bind to the liposomes, I found that this mutant caused a reduction in protein-liposome binding (Figure 36).

The K370E/R374E mutant with substitutions of positively charged amino-acid residues to negatively charged ones, decreased the binding between GAS7 proteins and liposomes, supporting the idea of the electrostatic interactions between the GAS7 and the membrane. I also

examined the non-tagged GAS7b K370E/R374E on liposome co-sedimentation assay. Unfortunately, I couldn't quantify the binding of proteins on the liposomes due to protein degradation. Our data showed that Q212, K370, and R374 amino-acid residues were the protein surface that interacts with the membrane surface.

a.

Proteins	Normal salt concentration		High salt concentration	
	+ Liposome	-Liposome	+ Liposome	-Liposome
GAS7b WT				
GAS7b K370E/R374E				

b.

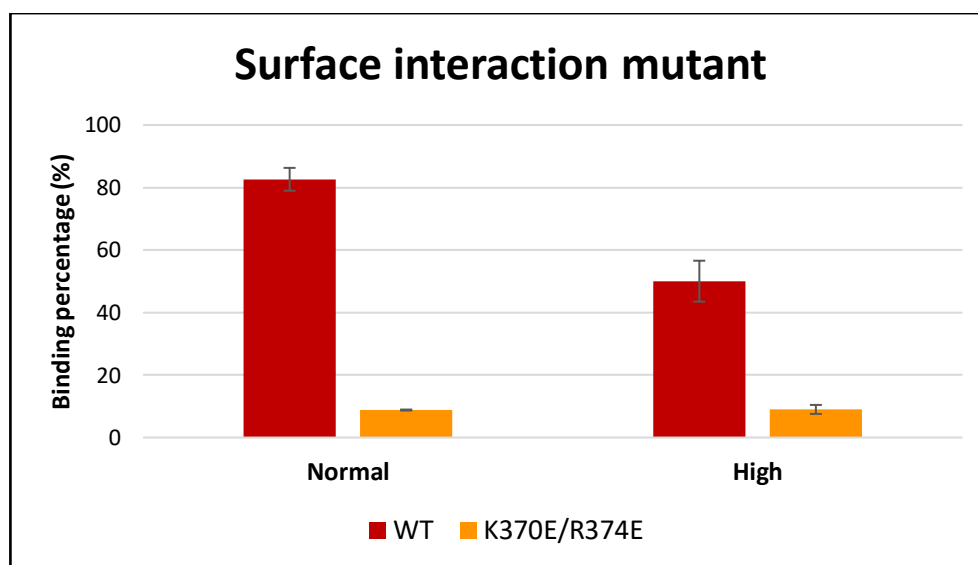


Figure 36: Liposome co-sedimentation assay, for surface interaction mutant. GFP-GAS7b WT and its mutation, K370E/R374E (0.5 μ M) were examined for their binding to liposome composed of total bovine brain lipid at normal (200 mM) and high salt concentration (300 mM). (a) Representative of the SDS-PAGE images from the assay. The presence of proteins in pellet (pt) indicates membrane binding. (b) Quantification of proteins in pellet from Figure 36a with liposomes. Sup: supernatant. N=3. Error bars: SD. The P-values were obtained by two-tailed Student's t-test. All isoforms are significant, $p < 0.01$, against the positive control.

3.3 Crosslinking assays

Crosslinking assay was carried out to examine the process of chemically joining two or more molecules (i.e. proteins) by a covalent bond. This assay could reveal low-resolution structural information for proteins, and novel information on protein-protein interaction. There are several considerations need to take to carry out, including the spacer arm length, the composition of the spacer arm, the spacer arm cleavability, and its solubility in the buffer. I selected BS(PEG)5 and Sulfo-EGS. Both reagents have the NHS ester reactive group. Table 4 shows the characteristics of these two reagents.

Table 4: Characteristics of the crosslinker reagents used in this study.

Reagent	Spacer arm length (Å)	Cleavability	Water soluble	Membrane permeability
BS(PEG)5	21.7	Not applicable	Yes	Nothing
Sulfo-EGS	16.1	Hydroxylamine	Yes	Nothing

Longer spacer arms will have greater flexibility and thus reduce steric hindrance. The cleavability refers to the ability of the reagent to break bonds that existed from the reactions between the proteins and crosslinkers, and to recover back the individual components.

I compared GFP-GAS7b WT, non-tagged GAS7b WT and non-tagged GAS7b R326A, at a protein concentration of 0.5 μ M, in the presence of different concentrations of the crosslinker reagents, BS(PEG)5 and Sulfo-EGS. After reaction with BS(PEG)5 or Sulfo-EGS, there were higher molecular-weight fractions, indicating the formation of oligomer (Figure 37 and Figure 38). As the concentration of both crosslinkers increased, there were increase in the amount of the higher molecular-weight fractions. The increased crosslinker reagents concentration were shown to increase the fraction consistent with the tetramer (tet) of non-tagged GAS7b WT, but this increase was not observed with the non-tagged GAS7b R326A. There was no difference in the fraction consistent with the dimer between non-tagged GAS7b and the R326A mutant. Therefore, GAS7b formed the oligomer through the assembly of the dimers, while the R326A mutant did not. There were several molecular weight fractions consistent with the dimers, presumably because intramolecularly crosslinked proteins could migrate in the gel differently due to different quaternary structures of the multidomain proteins stabilized by crosslinking. Figure 37 and Figure 38 show the representative of images of the GAS7 after reaction with different concentrations of BS(PEG)5 and Sulfo-EGS, respectively.

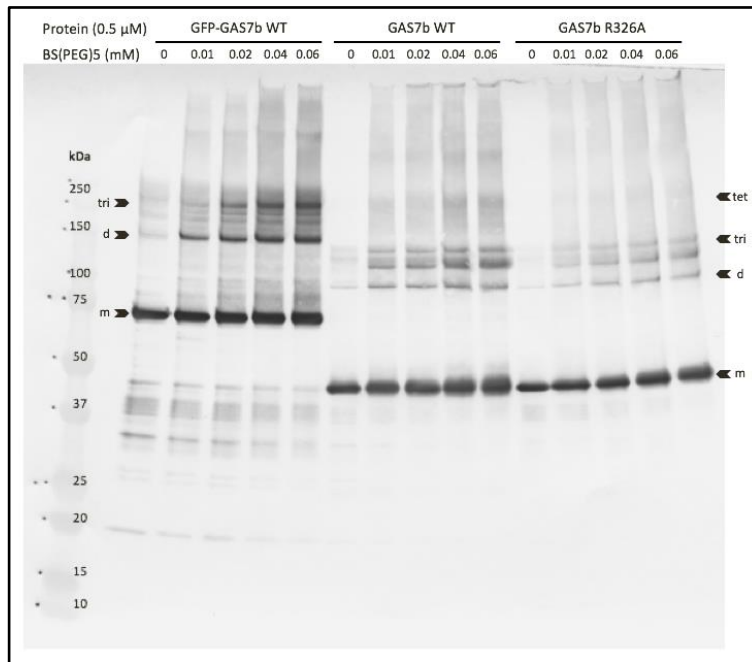


Figure 37: Western blot showing the comparison in the crosslinking assay of GFP-GAS7b WT, non-tagged GAS7b WT and non-tagged GAS7b R326A at different concentration of BS(PEG)5. The arrowed marked band represent tetramer (tet), trimer (tri), dimer (d) and monomer (m).

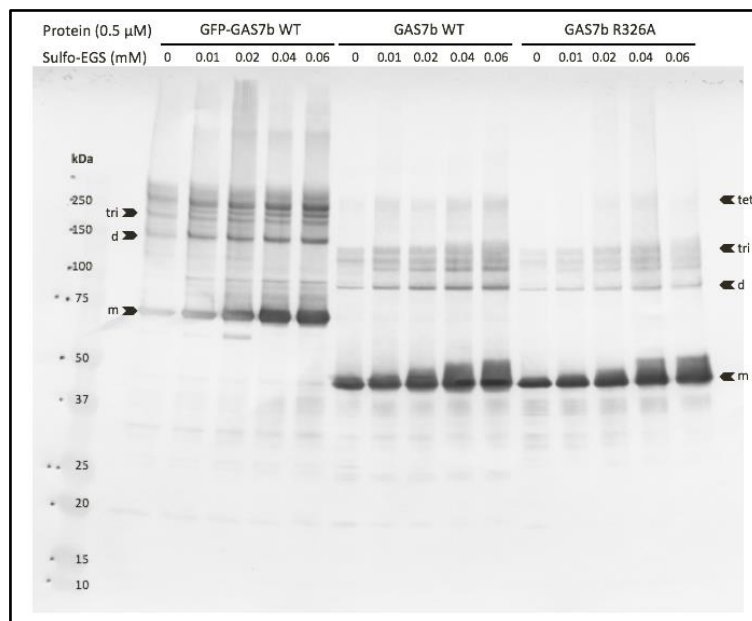


Figure 38: Western blot showing the comparison in the crosslinking assay of GFP-GAS7b WT, non-tagged GAS7b WT and non-tagged GAS7b R326A at different concentration of Sulfo-EGS. The arrowed marked band represent tetramer (tet), trimer (tri), dimer (d) and monomer (m).

Based on Figure 37 and Figure 38, non-tagged GAS7b WT showed a very clear tetramer band. Hence, I decided to further investigate the oligomer formation of non-tagged GAS7b WT on liposome, using both crosslinker reagents. The liposome that I used was bovine brain Folch. As shown in Figure 39, the increased of BS(PEG)5 concentrations increased the amount of the higher molecular-weight fractions. There were clear tetramer bands in the reactions with the presences of liposome, as compared to the reactions without liposome. However, the Sulfo-EGS crosslinker reagent was not able to show a clear band of trimer in the presence and absence of liposome (Figure 40). There was no tetramer band formed with this reagent. The difference in the trimer and tetramer bands formation from this both reagents are most probably due to the length of the spacer arm for each crosslinker. BS(PEG)5 consists longer spacer arm length as compared to Sulfo-EGS, thus BS(PEG)5 is more flexible to form a conjugate as compared to Sulfo-EGS. The formation of higher molecular-weight fractions in the presence of liposome strongly suggest that GAS7b was able to form oligomer on the liposome.

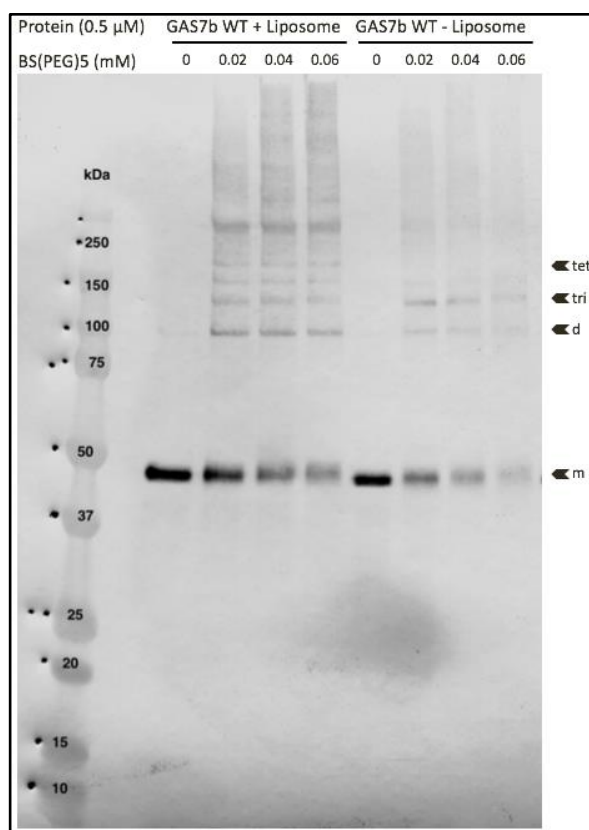


Figure 39: Western blot showing the comparison in the crosslinking assay of non-tagged GAS7b WT at different concentration of BS(PEG)5, in the presence and absence of liposome. The arrowed marked band represent tetramer (tet), trimer (tri), dimer (d) and monomer (m).

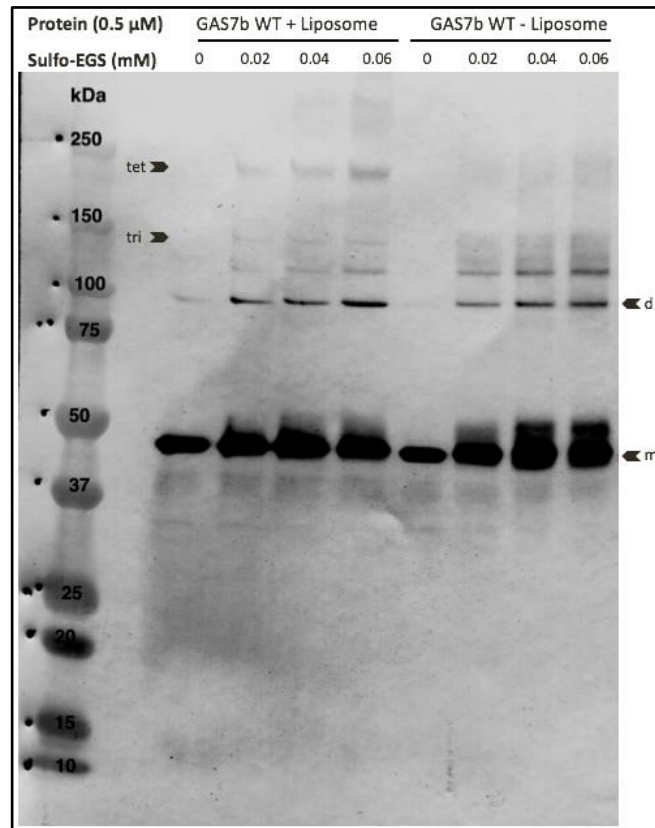


Figure 40: Western blot showing the comparison in the crosslinking assay of non-tagged GAS7b WT at different concentration of Sulfo-EGS, in the presence and absence of liposome. The arrowed marked band represent tetramer (tet), trimer (tri), dimer (d) and monomer (m).

4.0 Discussions

Protein-lipid interactions play important roles in cell signaling, lipid metabolism and membrane trafficking. Bin-Amphiphysin-Rvs167 (BAR) domains are highly conserved and play major roles in membrane curvature formation. The shape of the membranes changes during various conditions such as cell migration, cell division, endocytosis and phagocytosis (Itoh and Camilli, 2006; Tsujita *et al.*, 2006; Suetsugu *et al.*, 2014). There are three subfamilies in the BAR domain. The subfamilies are N-BAR/BAR, the F-BAR (extended Fes-CIP4 homology (EFC)/FCH-BAR) and the I-BAR (IRSp53-MIM homology domain protein/inverse-BAR) domains.

Growth-Arrest Specific 7 protein (GAS7) is one of the proteins in the F-BAR sub-family. GAS7 consists of the SH3 domain, the WW domain, and the F-BAR domain. It is the only protein in the F-BAR family, with its F-BAR located at the C-terminal.

In this study, I have found that all the GAS7 isoforms have high binding ability to the liposome. The binding of all the isoforms to the liposomes suggests that the location of the F-BAR domain in GAS7 at the C-terminal does not affect the liposome-binding properties. To determine the amino-acids residues in the F-BAR domain responsible for the binding ability, I introduced several mutations on the F-BAR domains by referring the crystal structure of the GAS7 F-BAR domain. The asymmetric unit of GAS7 F-BAR domain crystal structure consists of two dimers. These dimers interacted with symmetry-related dimers, forming oblique filamentous oligomers with flat surfaces in the crystals, to which I refer as flat filamentous oligomers (FFOs) (as shown in Figure 8c).

The F-BAR domain consists of two loops, which I refer as the filament forming loop 1 (FFL1) which is at amino-acid residues 171-197; and filament forming loop 2 (FFL2) which is at amino-acid residues 206-219. Based on our findings, both loops were shown to be involved in the formation of the FFO. In HeLa cells, the membrane binding of GAS7 as FFO was indicated by the GAS7b localization, where GAS7 excluded the plasma membrane marker, suggesting that GAS7 assembles into patches of highly concentrated GAS7b on the plasma membrane. In order to know the function of these loops, I deleted both of these FFLs and expressed these mutants in HeLa cells to examine their membrane localization. The deletion mutants of FFL1 and FFL2 showed significantly reduced patches formation as compared to the WT. This suggest that both FFL1 and FFL2 are involved in the patch formation in the HeLa cells. I also performed liposome co-sedimentation assay to examine the binding of these mutants on lipids. The membrane bindings of these deletion mutants with liposome were shown

to significantly decrease in the co-sedimentation assay. Therefore, I proposed that these loops are involved with the interaction between the adjacent dimers. The interaction between dimers will assemble to form oligomers on the membrane surface. Hence, when the assembly of these oligomers are hindered by the deletions, the formation of the protein oligomers on the membrane surface will also be prohibited, resulting in the reduced membrane binding activity. Our data had strongly suggest that GAS7 binds as oligomer to the membrane. An illustration of this hypothesis is shown in Figure 41.

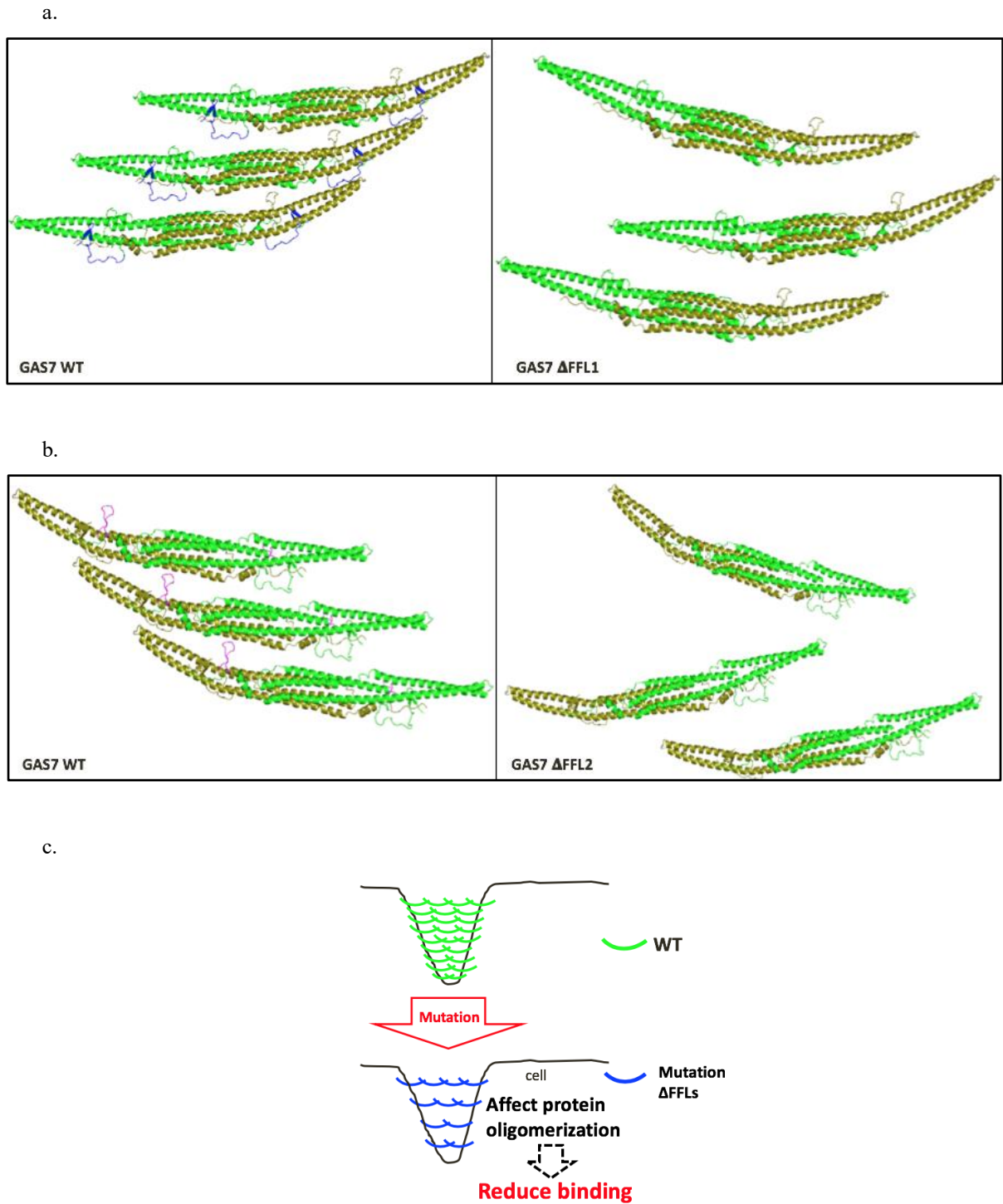


Figure 41: Illustration showing the hypothesis of the GAS7 oligomerization on membrane surface when both Δ FFLs were introduced. (a) Ribbon diagram of GAS7 crystal structure showing the comparison of oligomerization between the GAS7b WT and GAS7 Δ FFL1. (b) Ribbon diagram of GAS7 crystal structure showing the comparison of oligomerization between the GAS7b WT and GAS7 Δ FFL2. (c) Both FFLs are involved with the interaction between dimers. Thus, their deletion affected the protein oligomerization on membrane surface, and caused reduction in protein binding.

In reference to the GAS7 F-BAR domain crystal structure, one of the two FFL1 surface does not interact with the adjacent dimers in the FFO formation. Q212 is located at the tip of one of the FFL2 and is exposed to the surface of FFO. Hence, I mutated Q212, by replacing glutamine (Q); an uncharged amino acid, to arginine (R); a positively charged amino acid. Our *in vivo* assay showed that the Q212R mutant showed patches, which is similar as the WT in HeLa cells. Interestingly, the Q212R mutant increased the membrane binding in liposome co-sedimentation assay, in both normal and high salt concentration. The change in positive charge at this amino acid was suggested to increase the binding between the membrane surface and the proteins, as the membrane region are rich in anionic phospholipids. This is based on previous findings that had concluded the concave side of the F-BAR crescent-shaped dimer is positively charged and consists of conserved residues (Shimada *et al.*, 2007). Therefore, I proposed that this amino-acid residue, has a direct contact with the membrane surface and is suggested to be involved in the membrane binding. In addition, this data also indicates that this side of FFL2 does not involved in membrane insertion, which suggested that this FFL2 is hydrophilic. An illustration on how does this mutation works on the membrane binding is shown in Figure 42.

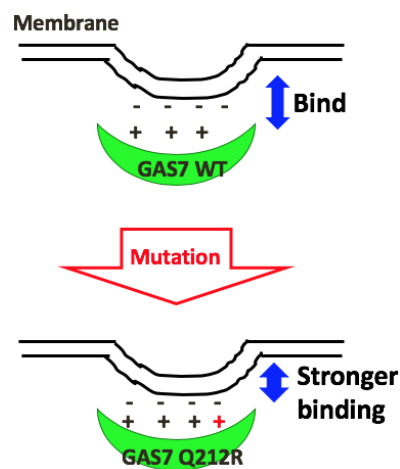


Figure 42: Illustration showing how Q212R mutation affected the binding in liposome co-sedimentation assay.

I found that R326 residue has contact sites with FFL1 and FFL2. The contact site in FFL1 is N177 and in FFL2 is D207. I proposed that this R326 residue might contribute to the stability of the FFLs. Hence, I substituted R326 to alanine, N177 to proline and D207 to arginine. Liposome co-sedimentation assay showed that N177P and D207R mutants significantly decreased the binding between proteins and lipids, both in normal and high salt concentrations. R326A also showed a significant decreased in binding in the normal salt concentration. However, in high salt concentration, the binding was not significantly decreased. This data

might refer to the other surface of the FFL2, which interacts with the membrane surface. This side was not affected by the R326A mutation, as much as it affected the FFL2 surface that interacts with the adjacent dimers. Thus, this strongly support that R326 plays important role in stabilizing the FFLs formation, making sure the interactions between this FFLs are intact to maintain the FFO formation. An illustration on how does these mutations work on the membrane binding is shown in Figure 43.

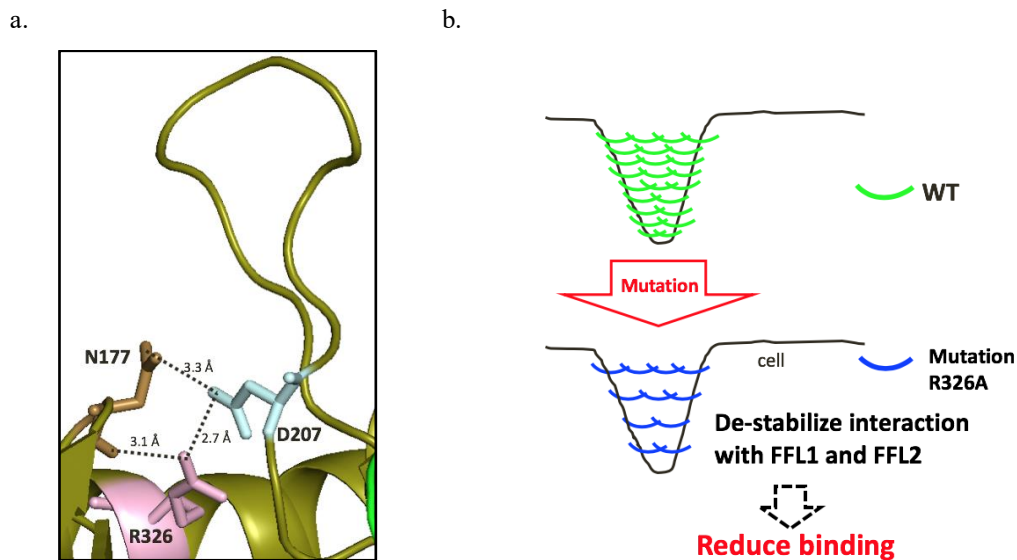


Figure 43: Illustration showing how R326A mutation affected the interaction between FFL1 and FFL2. (a) Ribbon diagram of GAS7 showing the interaction between R326 (lightpink) and both FFLs. N177 (sand) is located on FFL1 while D207 (palecyan) is located on FFL2. (b) The mutation done on R326 was suggested to de-stabilize the interaction between FFL1 and FFL2, thus affecting the binding between the protein and lipids in liposome co-sedimentation assay.

K370E/R374E mutation was also suggested to be involved with the interaction between the membrane surface and the proteins, thus I named them as the surface interaction mutant, same as Q212R. These residues are located on the oligomer surface. Accordingly, the replacement of positively charged amino acid lysine in 370 and arginine in 374 to negatively charged glutamic acid, had greatly reduced the binding between the F-BAR domains and the membrane surface. This suggest that K370/R374 interacts directly with the membrane surface, thus the change in the amino acid charge affected the binding towards the membrane. An illustration on how does this mutation works on the membrane binding is shown in Figure 44.

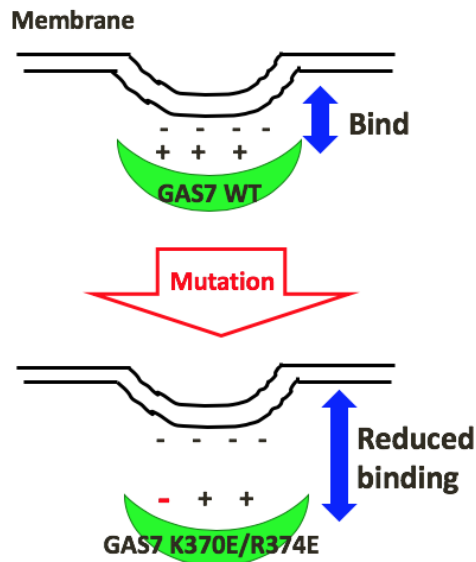
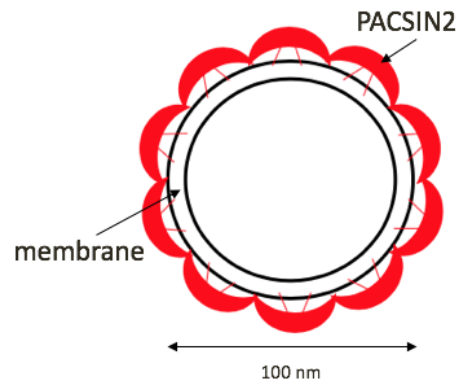


Figure 44: Illustration showing how K370E/R374E mutation affected the binding in liposome co-sedimentation assay.

Based on these data, I propose the mechanism of GAS7 binding to the membrane is different from other F-BAR domains of PACSIN2 and CIP4. In PACSIN2, the wedge loop at its F-BAR domain are hydrophobic (as shown in Figure 6) and are inserted into the membrane. The insertion into the membrane bilayer as wedge, helps PACSIN2 to form curvature on the membrane (Wang *et al.*, 2009; Shimada *et al.*, 2010; Senju *et al.*, 2011) (as shown in Figure 10). The analysis of the crystal packing of PACSIN2 showed that tip-to-tip interaction may also contributed to the PACSIN2 packing on membrane (Bai and Zheng, 2013). The elimination of this tip-to-tip interaction inhibits the tubulation function of PACSIN2 by affecting the number, diameter and length of tubules. The binding of PACSIN2 around the membrane tubules was shown to be in putative oligomeric spiral form (Bai and Zheng, 2013; Senju and Suetsugu, 2015) (Figure 45a). This formation can be seen the caveolae formation (Figure 45b).

a.



b.

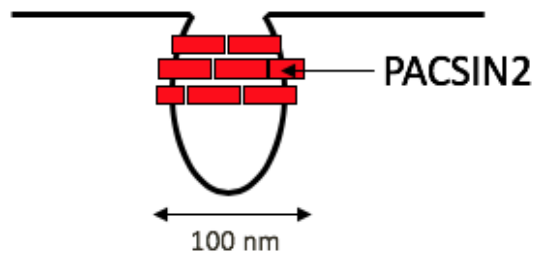


Figure 45: Structure of PACSIN2 F-BAR domain crystal structure. (a) Illustration showing the putative oligomeric spiral of PACSIN2 F-BAR domain around membrane tubules. (b) The putative oligomeric spiral of PACSIN2 F-BAR domain found in the formation of caveolae.

As compared to our findings, GAS7 loops were hydrophilic, hence, no membrane insertion occurs for the membrane binding. The loops in GAS7 were shown to be involved in the protein oligomerization and membrane surface interaction. An illustration of the comparison between these loops from these two proteins are shown in Figure 46.

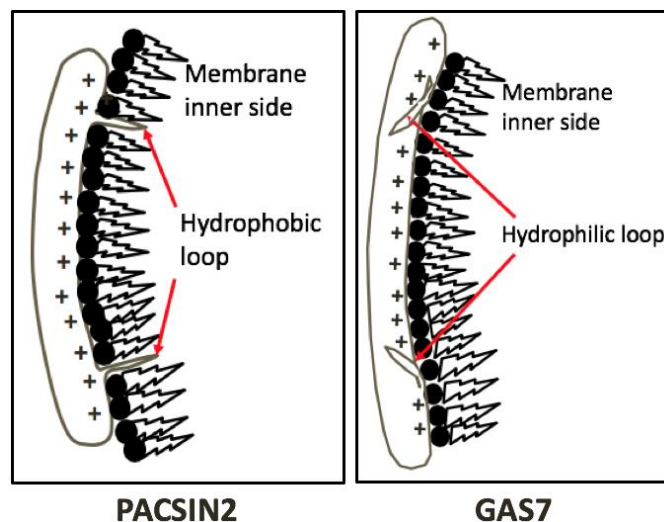


Figure 46: Illustrations show the difference mechanisms of PACSIN2 (left) and GAS7 (right) bind on membrane surface.

On the other hand, I-BAR protein, Pinkbar, does not induce any membrane protrusions or invagination. It also does not tubulate membrane. Instead, it promotes the formation of planar membrane sheets by deforming phosphoinositide-rich membranes (Pykäläinen *et al.*, 2011). The N-terminal α -helix of the BAR domain Pinkbar are inserted into the membrane bilayer, which sense and generate negative curvature (Figure 47).

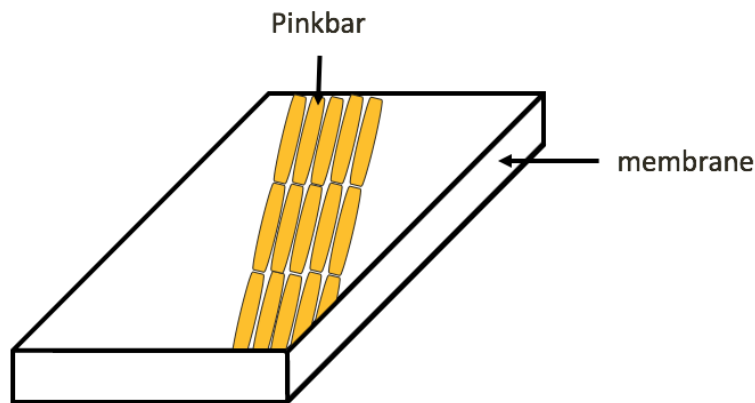


Figure 47: The membrane-binding surfaces of individual Pinkbar domains all face in the same direction in the planar oligomer of the crystal lattice and thus the lipid-binding interface in the oligomer is relatively flat.

As for GAS7 F-BAR domain, the interaction between dimers through FFL1 and FFL2 will assemble the F-BAR domains to form oligomers on the membrane surface. When the assembly of these oligomers is hindered by the deletions, the formation of the protein oligomers on the membrane surface will also be inhibited. This resulted in the reduced membrane binding activity, and was proven by co-sedimentation assay. The mutation of R326 might affect the location of the two FFLs, and thereby change the stability of the oligomer formation through the loops. This had affected the oligomer formation in the cells or on the membrane, because the R326 mutant retained the membrane binding *in vitro* without the patch assembly in the HeLa cells. The reduction in the band intensity in the crosslinking assays showed that GAS7 R326A was not able to form oligomers as compared to GAS7b WT. Based on this data, I proposed that the FFLs contribute to the formation of oligomers that can further assemble into sheets along the membrane surface. These sheets might actually be involved in the lamellipodia formation of migrating cells. An illustration on how does the sheets assemble on the membrane is shown in Figure 48.

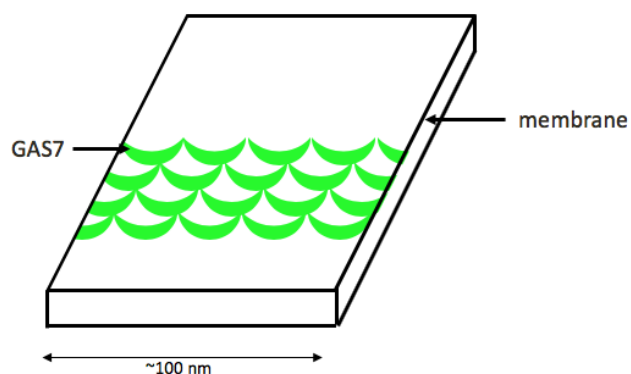


Figure 48: Illustration on how does the GAS7 F-BAR domain (green) assembles on the membrane to form sheets.

In this study, I have shown the binding mechanism of GAS7 on the membrane. The loops region in GAS7 F-BAR domain crystal structure was shown to be hydrophilic, thus I proposed that these loops were not involved in membrane insertion. The formation of oligomers by the FFLs also has shown that this protein assembles on the membrane surface by forming sheets.

5.0 Acknowledgments

I would like to take this opportunity to thank those who have helped me to finally complete this GAS7 project.

Firstly, I would like to express my biggest gratitude to my supervisor, Prof Dr Shiro Suetsugu, for all his guidance, critics, comments, supports and most importantly, his patience, in helping me throughout the past three years in finishing this GAS7 project. Without his help, I don't think I would be able to finish this project successfully. I also want to thank both of my laboratory Assistant Professors, Dr Kyoko Hanawa-Suetsugu and Dr Tamako Nishimura, for helping me to troubleshoot most of the experiments that I had problems with.

Thank you to both of my PhD advisors, Prof Dr Toshio Hakoshima and Prof Dr Tomoya Tsukazaki, for all their advices, suggestions and comments during my studies.

This project was also a collaboration project with few research institutes. Hence, I would like to take this opportunity to thank Prof Dr. Daisuke Kohda and Associate Prof Dr. Atsushi Shimada from Medical Institute of Bioregulation, Kyushu University and RIKEN Spring-8 Center, for the GAS7 F-BAR domain crystal structure. I also want to thank Dr Naoyuki Miyazaki and Dr Kenji Iwasaki, both from Institute for Protein Research, Osaka University, for helping me in obtaining the best cryo-EM images.

I want to acknowledge MEXT for sponsoring my studies in Japan for three years. To the international committee of NAIST-BIO, especially Dr Satoko Maki, for all her efforts in giving opportunities to international students, especially from South East Asia, to study here.

A big thanks to both of my parents, who have been my main moral support from the moment I came here for internship until I finally completed my doctoral program. Thank you to my families and friends (especially Kamila, Aisyah and Aidil) who have been constantly praying and wishing the best for me in finishing up my studies until the end.

Lastly, thank you to all the lab members of Suetsugu's laboratory, from batch 2014/2015 until the current batch. Thank you too to those who had helped me in this project.

Thank you.

6.0 References

Abbott, M-A., Wells, D. G., and Fallon, J. R. (1999). The insulin receptor tyrosine kinase substrate p58/53 and the insulin receptor are components of CNS synapses. *The Journal of Neuroscience* 19(17), 7300-7308.

Ahmed, S., Bu, W., Lee., R. P. T., Maurer-Stroh, S., and Goh, W. I. (2010). F-BAR domain proteins: Families and functions. *Communicative & Integrative Biology* 3(2), 116-121.

Alam Shibly, S. U., Ghatak, C., Sayem Karai, M. A., Moniruzzaman, M., and Yamazaki, M. (2016). Experimental estimation of membrane tension induced by osmotic pressure. *Biophysical Journal* 111(10), 2190-2201.

Arkipov, A., Yin, Y., and Schulten, K. (2009). Membrane-bending mechanism of amphiphysin N-BAR domains. *Biophysical Journal* 97(10), 2727-2735.

Ayton, G. S., Blood, P. D., and Voth, G. A. (2007). Membrane remodeling from N-BAR domain interactions: Insights from multi-scale simulation. *Biophysical Journal* 92(10), 3595-3602.

Ayton, G. S., Lyman, E., Krishna, V., Swenson, R. D., Mim, C., Unger, V. M., and Voth, G. A. (2009). New insights into BAR domain-induced membrane remodeling. *Biophysical Journal* 97(6), 1616-1625.

Bai, X., and Zheng, X. (2013). Tip-to-tip interaction in the crystal packing of PACSIN2 is important in regulating tubulation activity. *Protein & Cell* 4(9), 695-701.

Campelo, F., Fabrikant, G., McMahon, H. T., and Kozlov, M. M. (2009). Modeling membrane shaping by proteins: Focus on EHD2 and N-BAR domains. *FEBS letters* 584(9), 1830-1839.

Castellano, F. Chavrier, P., and Caron, E. (2001). Actin dynamics during phagocytosis. *Immunology* 13, 347-355.

- Chang, P. Y., Kuo, J. T., Lin-Chao, S., and Chao, C. C. (2005). Identification of rat GAS7 isoforms differentially expressed in brain and regulated following kainate-induced neuronal injury. *Journal of Neuroscience Research* 79(6), 788-797.
- Chen, Z., Chang, K., Capraro, B. R., Zhu, C., Hsu, C. J., and Baumgart, T. (2014). Intradimer/Intermolecular interactions suggest autoinhibition mechanism in endophilin A1. *Journal of the American Chemical Society* 136(12), 4557-4564.
- Chen, Z., Zhu, C., Kuo, C. J., Robustelli, J., and Baumgart, T. (2016). The N-terminal amphipathic helix of endophilin does not contribute to its molecular curvature generation capacity. *Journal of The American Chemical Society* 138(44), 14616-14622.
- Choi, J., Ko, J., Racz, B., Burette, A., Lee, J-R., Kim, S., Na, M., Lee, H. W., Kim, K., Weinberg, R. J., and Kim, E. (2005). Regulation of dendritic spine morphogenesis by insulin receptor substrate 53, a downstream effector of Rac1 and CDC42 small GTPases. *The Journal of Neuroscience* 25(4), 869-879.
- Chong, P. A., Lin, H., Wrana, J. L., and Forman-Kay, J. D. (2006). An expanded WW domain recognition motif revealed by the interaction between Smad7 and the E3 ubiquitin ligase Smurf2. *The Journal of Biological Chemistry* 281(25), 17069-17075.
- Cui, H., Ayton, G. S., and Voth, G. A. (2009). Membrane binding by the endophilin N-BAR domain. *Biophysical Journal* 97(10), 2746-2753.
- Daumke, O., Roux, A., and Haucke, V. (2014). BAR domain scaffolds in dynamin-mediated membrane fission. *Cell* 156(5), 882-892.
- Frolov, V. A., and Zimmerberg, J. (2008). Flexible scaffolding made of rigid BARs. *Cell* 132(5), 727-729.
- Frost, A., De Camilli, P., and Unger, V. M. (2007). F-BAR proteins join the BAR family fold. *Structure* 15(7), 751-753.

Frost, A., Perere, R., Roux, A., Spasov, K., Destaing, O., Egelman, E. H., Camilli, P. D., and Unger, V. M. (2008). Structural basis of membrane invagination by F-BAR domains. *Cell* 132(5), 807-817.

Frost, A., Unger, V. M., and De Camilli, P. (2009). The BAR domain superfamily: Membrane-molding macromolecules. *Cell* 137, 191-196.

Gallop, J. L., Jao, C. C., Kent, H. M., Butler, P. J., Evans, P. R., Langen, R., and McMahon, H. T. (2006). Mechanism of endophilin N-BAR domain-mediated membrane curvature. *The EMBO Journal* 25(12), 2663-2952.

Gotoh, A., Hidaka, M., Hirose, K., and Uchida, T. (2013). Gas7b (Growth Arrest Specific 7B) regulates neuronal cell morphology by enhancing microtubules and actin filament assembly. *The Journal of Biological Chemistry* 288(48), 34699-34706.

Govind, S., Kozma, R., Monfries, C., Lim, L., and Ahmed, S. (2001). Cdc42Hs facilitates cytoskeletal reorganization and neurite outgrowth by localizing the 58-kD insulin receptor substrate to filamentous actin. *The Journal of Cell Biology* 153(3), 579-594.

Habermann, B. (2004). The BAR-domain family of proteins: a case of bending and binding. *Embo Reports* 5(3), 250-255.

Heath, R. J. W., and Insall, R. H. (2008). F-BAR domains: multifunctional regulators of membrane curvature. *Journal of Cell Science* 121(pt2), 1951-1954.

Henne, W. M., Kent, H. M., Ford, M. G., Hegde, B. G., Daumke, O., Butler, P. J., Mittai, R., Langen, R., Evans, P. R., and McMahon, H. T. (2007). Structure and analysis of FCHO2 F-BAR domain: A dimerizing and membrane recruitment module that effects membrane curvature. *Structure* 15(7), 839-852.

Henne, W. M., Boucrot, E., Meinecke, M., Evergren, E., Vallis, Y., Mittai, R., and McMahon, H. T. (2010). FCHO proteins are nucleators of clathrin-mediated endocytosis. *Science* 328(5983), 1281-1284.

Hidaka, M., Koga, T., Gotoh, A., Sanada, M., Hirose, K., and Uchida, T. (2012). Alzheimer's disease-related protein hGas7b interferes with kinesin motility. *The Journal of Biochemistry* 151(6), 593-598.

Ingham, R. J., Colwill, K., Howard, C., Dettweiler, S., Lim, C. S., Yu, J., Hersi, K., Raajimakers, J., Gish, G., *et al* (2005). WW domains provide a platform for the assembly of multiprotein networks. *Molecular and Cellular Biology* 25(16), 7092-7106.

Inaba, T., Kishimoto, T., Murate, M., Tajima, T., Sakai, S., Abe, M., Makino, A., Tomishige, N., Ishitsuka, R., Ikeda, Y., Takeoka, S., and Kobayashi, T. (2016). Phospholipase C β 1 induces membrane tubulation and is involved in caveolae formation. *PNAS* 113(28), 7834-7839.

Isas, J. M., Ambroso, M. R., Hegde, P. B., Langen, J., and Langen, R. (2015). Tubulation by amphiphysin requires concentration-dependent switching from wedging to scaffolding. *Structure* 23(5), 873-881.

Itoh, T., and Camilli, P. D. (2006). BAR, F-BAR (EFC) and ENTH/ANTH domains in the regulation of membrane-cytosol interfaces and membrane curvature. *Biochimica et Biophysica Acta* 1761(8), 897-912.

Li, J., Nishizawa, K., An, W., Hussey, R. E., Lialios, F. E., Salgia, R., Sunder-Plassmann, R., and Reinherz, E. L. (1998). A cdc15-like adaptor protein (CD2BP1) interacts with the CD2 cytoplasmic domain and regulates CD2-triggered adhesion. *The EMBO Journal* 17(24), 7320-7336.

Lim, K. B., Bu, W., Goh, W. I., Koh, E., Ong, S. H., Pawson, T., Sudhakaran, T., and Ahmed, S. (2008). The Cdc42 effector IRSp53 generates filopodia by coupling membrane protrusion with actin dynamics. *The Journal of Biological Chemistry* 283(29), 20454-20472.

Liu, P-S., Jong, T-H., Maa, M-C., and Leu, T-H. (2010). The interplay between Eps8 and IRSp53 contributes to Src-mediated transformation. *Oncogene* 29(27), 3977-3989.

Liu, S., Xiong, X., Zhao, X., Yang, X., and Wang, H. (2015). F-BAR family proteins, emerging regulators for cell membrane dynamic changes-from structure to human diseases. *Journal of Hematology & Oncology* 8(47). DOI 10.1186/s13045-015-0144-2

Macias, M. J., Wiesner, S., and Sudol, M. (2002). WW and SH3 domains, two different scaffolds to recognize proline-rich ligands. *FEBS letter* 513(1), 30-37.

Mattila, P. K., Pykäläinen, A., Saarikangas, J., Paavilainen, V. O., Vihinen, H., Jokitalo, E., and Lappalainen, P. (2007). Missing-in-metastasis and IRSp53 deform PI(4,5)P₂-rich membranes by an inverse BAR domain-like mechanism. *Journal of Cell Biology* 176(7), 953-964.

Meer, G. V., Voelker, D. R., and Feigenson, G. W. (2008). Membrane lipids: Where they are and how they behave. *Nature Reviews Molecular Cell Biology* 9(2), 112-124.

Michelsen, P., Jergil, B., and Odham, G. (1995). Quantification of polyphosphoinositides using selected ion monitoring electrospray mass spectrometry. *Rapid Communications in Mass Spectrometry* 9(12), 1109-1114.

Mim, C., Cui, H., Gawronski-Salerno, J. A., Frost, A., Lyman, E., Voth, G. A., and Unger, V. M. (2012). Structural basis of membrane bending by the N-BAR protein endophilin. *Cell* 149(1), 137-145.

Nishimura, T., Morone, N., and Suetsugu, S. (2018). Membrane re-modelling by BAR domain superfamily proteins via molecular and non-molecular factors. *Biochemical Society Transactions* 46(2), 379-389.

Peter, B. J., Kent, H. M., Millis, I. G., Vallis, Y., Butler, P. J., Evans, P. R., and McMahon, H. T. (2004). BAR domains as sensors of membrane curvature: The amphiphysin BAR structure. *Science* 303(5657), 495-499.

Pykäläinen, A., Boczkowska, M., Zhao, H., Saarikangas, J., Rebowski, G., Jansen, M., Hakanen, J., *et al* (2011). Pinkbar is an epithelial-specific BAR domain protein that

generates planar membrane structures. *Nature Structural & Molecular Biology* 18(8), 902-908.

Qualmann, B., and Kelly, R. B. (2000). Syndapin isoforms participate in receptor-mediated endocytosis and actin organization. *The Journal of Cell Biology* 148(5), 1047-1061.

Qualmann, B., Koch, D., and Kessels, M. M. (2011). Let's go bananas: Revisiting the endocytic BAR code. *The EMBO Journal* 30(17), 3501-3515.

Rao, Y., Ma, Q., Vahedi-Faridi, A., Sundborger, A., Pechstein, A., Puchkov, D., Luo, L., *et al* (2010). Molecular basis for SH3 domain regulation of F-BAR-mediated membrane deformation. *PNAS* 107(18), 8213-8218.

Robens, J. M., Yeow-Fong, L., Ng, E., Hall, C., and Manser, E. (2010). Regulation of IRSp53-dependent filopodial dynamics by antagonism between 14-3-3 binding and SH3-mediated localization. *Molecular and Cellular Biology* 30(3), 829-844.

Safari, F., and Suetsugu, S. (2012). The BAR Domain superfamily proteins from subcellular structures to human diseases. *Membranes* 2(1), 91-117.

Salzer, U., Kostan, J., and Djjinovic'-Carugo, K. (2017). Deciphering the BAR code of the membrane modulators. *Cellular and Molecular Life Sciences* 74(13), 2413-2438.

Scita, G., Confalonieri, S., Lappalainen, P., and Suetsugu, S. (2008). IRSp53: crossing the road of membrane and actin dynamics in the formation of membrane protrusions. *Trends in Cell Biology* 18(2), 52-60.

Senju, Y., Itoh, Y., Takano, K., Hamada, S., and Suetsugu, S. (2011). Essential role of PACSIN2/syndapin-II in caveolae membrane sculpting. *Journal of Cell Science* 124(pt12), 2032-2040.

Senju, Y., and Suetsugu, S. (2015). Possible regulation of caveolar endocytosis and flattening by phosphorylation of F-BAR domain protein PACSIN2/Syndapin II. *BioArchitecture* 5(5-6), 70-77.

She, B-R., Liou, G-G., and Lin-Chao, S. (2002). Association of the Growth-Arrest-Specific Protein Gas7 with F-actin induces reorganization of microfilaments and promotes membrane outgrowth. *Experimental Cell Research* 273(1), 34-44.

Shimada, A., Niwa, H., Tsujita, K., Suetsugu, S., Nitta, K., Hanawa-suetsugu, K., Akasaka, R., *et al* (2007). Curved EFC/F-bar domain dimers are joined end to end into a filament for membrane invagination in endocytosis. *Cell* 129(4), 761-772.

Shimada, A., Takano, K., Shirouzu, M., Hanawa-Suetsugu, K., Terada, T., Toyooka, K., Umehara, T., Yamamoto, M., Yokoyama, S., and Suetsugu, S. (2010). Mapping of the basic amino-acid residues responsible for tabulation and cellular protrusion by the EFC/F-BAR domain of pacsin2/Syndapin II. *FEBS letters* 584(6), 1111-1118.

Simunovic, M., Voth, G. A., Callan-Jones, A., and Bassereau, P. (2015). When physics takes over: BAR proteins and membrane curvature. *Trends in Cell Biology* 25(12), 78-792.

Soltau, M., Richter, D., and Kreienkamp, H-J. (2002). The insulin receptor substrate IRSp53 links postsynaptic shank1 to the small G-protein cdc42. *Molecular and Cellular Neuroscience* 21(4), 575-583.

Soltau, M., Berhorster, K., Kindler, S., Buck, F., Richter, D., and Kreienkamp, H-J. (2004). Insulin receptor substrate of 53 kDa links postsynaptic shank to PSD-95. *Journal of Neurochemistry* 90(3), 659-665.

Spencer, S., Dowbenko, D., Cheng, J., Li, W., Brush, J., Utzig, S., Simanis, V., and Lasky, L. A. (1997). PSTPIP: A tyrosine phosphorylated cleavage furrow-associated protein that is a substrate for a PEST tyrosine phosphatase. *The Journal of Cell Biology* 138(4), 845-860.

Suetsugu, S., Murayama, K., Sakamoto, A., Hanawa-Suetsugu, K., Seto, A., Oikawa, T., Mishima, C., Shirouzu, M., Takenawa, T., and Yokoyama, S. (2006a). The RAC binding domain/IRSp53-MIM homology domain of IRSp53 induces RAC-dependent membrane deformation. *The journal of Biological Chemistry* 281(46), 35347-35358.

Suetsugu, S., Kurisu, S., Oikawa, T., Yamazaki, D., Oda, A., and Takenawa, T. (2006b). Optimization of WAVE2 complex-induced actin polymerization by membrane-bound IRSp53, PIP₃, and Rac. *The Journal of Cell Biology* 173(4), 571-585.

Suetsugu, S., Toyooka, K., and Senju, Y. (2010). Subcellular membrane curvature mediated by the BAR domain superfamily proteins. *Seminars in Cell & Developmental Biology* 21(4), 340-349.

Suetsugu, S., and Gautreau, A. (2012). Synergistic BAR-NPF interactions in actin-driven membrane remodeling. *Trends in Cell Biology* 22(3), 141-150.

Suetsugu, S., Kurisu, S., and Takenawa, T. (2014). Dynamic shaping of cellular membranes by phospholipids and membrane-deforming proteins. *Physiological Reviews* 94(4), 1219-1248.

Suetsugu, S. (2016). Higher-order assemblies of BAR domain proteins for shaping membranes. *Microscopy* 65(3), 201-210.

Tseng, R. C., Chang, J. W., Mao, J. S., Tsai, C. D., Wu, P. C., Lin, C. J., Lu, Y. L., Liao, S. Y., Cheng, H. C., Hsu, H. S., and Wang, Y. C. (2015). Growth-arrest-specific 7C protein inhibits tumor metastasis via the N-WASP/FAK/F-actin and hnRNP U/ β -TrCP/ β -catenin pathways in lung cancer. *Oncotarget* 6(42), 44207-44221.

Tsujita, K., Suetsugu, S., Sasaki, N., Furutani, M., Oikawa, T., and Takenawa, T. (2006). Coordination between the actin cytoskeleton and membrane deformation by a novel membrane tabulation domain of PCH proteins is involved in endocytosis. *The Journal of Cell Biology* 172(2), 269-279.

Wang, Q., Navarro, M. V., Peng, G., Molineli, E., Goh, S. L., Judson, B. L., Rajashankar, K. R., and Sondermann, H. (2009). Molecular mechanism of the membrane constriction and tabulation mediated by the F-BAR protein Pacsin/Syndapin. *PNAS* 106(31), 12700-12706

Wu, Y., Spencer, S. D., and Lasky, L. A. (1998a). Tyrosine phosphorylation regulates the SH3-mediated binding of the Wiskott-Aldrich Syndrome protein to PSTPIP, a cytoskeletal-associated protein. *The Journal of Biological Chemistry* 273(10), 5765-5770.

Wu, Y., Dowbenko, D., and Lasky, L. A. (1998b). PSTPIP 2, a second tyrosine phosphorylated, cytoskeletal-associated protein that binds a PEST-type protein-tyrosine phosphatase. *The Journal of Biological Chemistry* 273(46), 30487-30496.

Yin, Y., Arkhipov, A., and Schulten, K. (2009). Simulations of the membrane tubulation by lattices of amphiphysin N-BAR domains. *Structure* 17(6), 882-892.

You, J. J., and Lin-Chao, S. (2010). Gas7 functions with N-WASP to regulate the neurite outgrowth of hippocampal neurons. *The Journal of Biological Chemistry* 285(15), 11652-11666.

Zimmerberg, J., and Kozlov, M. M. (2006). How proteins produce cellular membrane curvature. *Nature Reviews Molecular Cell Biology* 7(2), 9-19.